SPECULAR REFLECTANCE OF ANODIZED 6061-T6 ALUMINUM ALLOY

by

JON STRAUSS

B.S., Oregon State University, 1998

A REPORT

submitted in partial fulfillment of the requirements for the degree

MASTER OF SCIENCE

Department of Chemical Engineering
College of Engineering

KANSAS STATE UNIVERSITY
Manhattan, Kansas

2013

Approved by:

Major Professor
Dr. John Schlup

Copyright

Abstract

This study investigated the specular reflectance properties of 6061-T6 aluminum alloy anodized in accordance with military specification MIL-A-8625 as a function of both etch process time and anodization process potential. Both process parameters affect the specular reflectance characteristics when measured using a 660 nm, collimated diode laser source. The etch process time, when varied between 0.5 to 20 minutes, resulted in a decrease in specular reflectivity with increasing time. The anodization process potential was varied between 10 and 21 volts, with a 15 volt condition producing samples with the greatest specular reflectivity. Between the two parameters, the etch time had the greater effect. Additionally, the dependence of the incident beam angle on specular reflectivity was shown not to have a significant effect when compared to the etch process time and process potential.

Table of Contents

List of Figures

List of Tables

Acknowledgements

I would like to express my gratitude to the many individuals who helped make this investigation possible. Foremost among them include my family, whose ardent support provided the motivation to finish. I would also like to express my appreciation to Mike Robinson and Diode Laser Concepts, Inc., who contributed resources and provided space to work. In addition, I am grateful for Diode Laser Concepts, Inc.'s engineering staff for providing needed technical dialogue and discussion. Finally, my thanks go to Dr. Schlup for his assistance and insight in the preparation of this report.

Chapter 1 - Introduction

Background: Diode Laser Concepts, Inc. Interest

Managing stray light is a key design consideration for developing laser diode modules. Diode Laser Concepts, Inc (DLC), a manufacturer of laser diode modules and systems is facing increased pressure to reduce artifacts caused by stray light. This presents a challenge for the company to meet customer demands while retaining competitively priced products. Consequently, DLC sustains an ongoing effort to develop innovative solutions to reduce, capture, or otherwise lessen the effect of stray light without adding significant cost to its products.

The typical DLC module design includes a diode laser source coupled with a focusing lens and other beam shaping optical elements, all mounted within a cylindrical, machined aluminum housing. The general concept of the design is shown below in Figure 1.1. This basic architecture provides an inexpensive, configurable platform for module design. However, as illustrated, any stray light that escapes the optical pathway has a tendency to reflect off of the machined aluminum surfaces. The reflected light then propagates through the system in an uncontrolled manner. If the light is able to escape the confines of the optical cavity, it may result in spot, ring, line or other undesirable optical images. An example is shown in Figure 1.2, which displays a near-field image projected by a laser module onto a viewing card 3 inches from the exit aperture. As indicated, the curved artifacts on either side of the central beam are caused by stray light. These and other artifacts may be detrimental to customer applications.

Figure 1.1: Diode Laser Module Concept Design

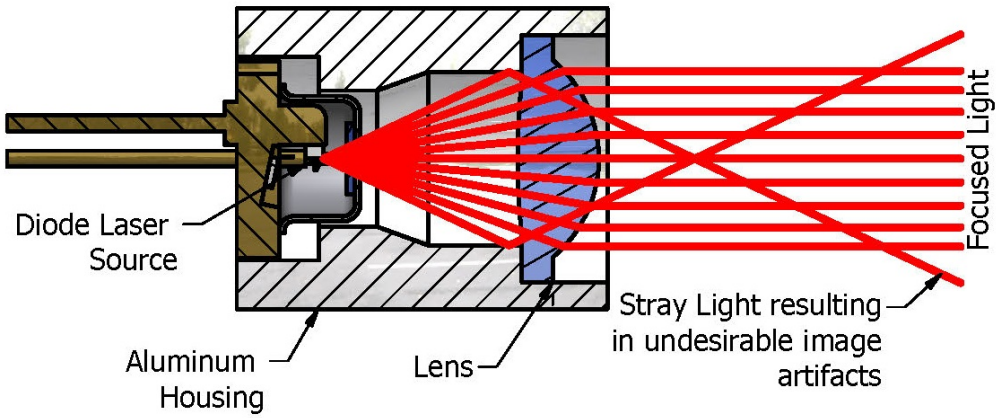

Figure 1.2: Stray Light Artifacts

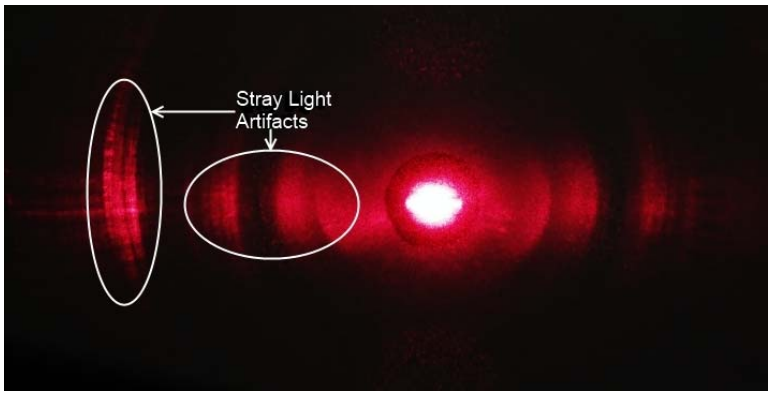

Methods employed by DLC for managing stray light are various and include mechanical design features, strategic use of apertures, optical element design, optical element placement, internal surface roughening, and coating reflective surfaces. The mechanisms may be generally divided into four categories 1) reduction of stray light by utilizing a design that minimizes the amount of stray light escaping the optical pathway, 2) capturing stray light and reflecting it in a controlled manner to minimize the impact on the optical image, 3) increasing the absorption characteristics of reflective surfaces, and 4) scattering reflected light to transform an intense specular reflection into a diffuse scattered reflection, thereby reducing the reflected optical power at any given point. Of these categories, the first three have received the greatest historical attention at DLC as they are the easiest to control with the company's processing capabilities. However, recently the fourth category has received interest for particularly demanding product specifications.

Specular Reflectivity

In response, DLC is interested in modifying surface characteristics of the machined aluminum housing with the goal of minimizing specular reflections. The concept focuses on the third and fourth categories listed above and is shown graphically in Figure 1.3. As shown, a specular reflection results when an incident ray of light is reflected off of a smooth surface in a single well-defined ray in the outgoing direction.[1,2] Conversely, when a ray is reflected from a rough surface, the light is scattered, resulting in a diffuse reflection. In addition, some fraction of the light is not reflected, but absorbed into the housing although with aluminum the absorbed fraction is generally low for wavelengths in the visible spectrum.[1] For the general DLC design,

either of these latter two phenomena, diffuse reflection or absorption, are desirable as they lessen the intensity of image artifacts caused by light reflected from the aluminum surfaces adjacent to the optical pathway.

Figure 1.3: Reflection

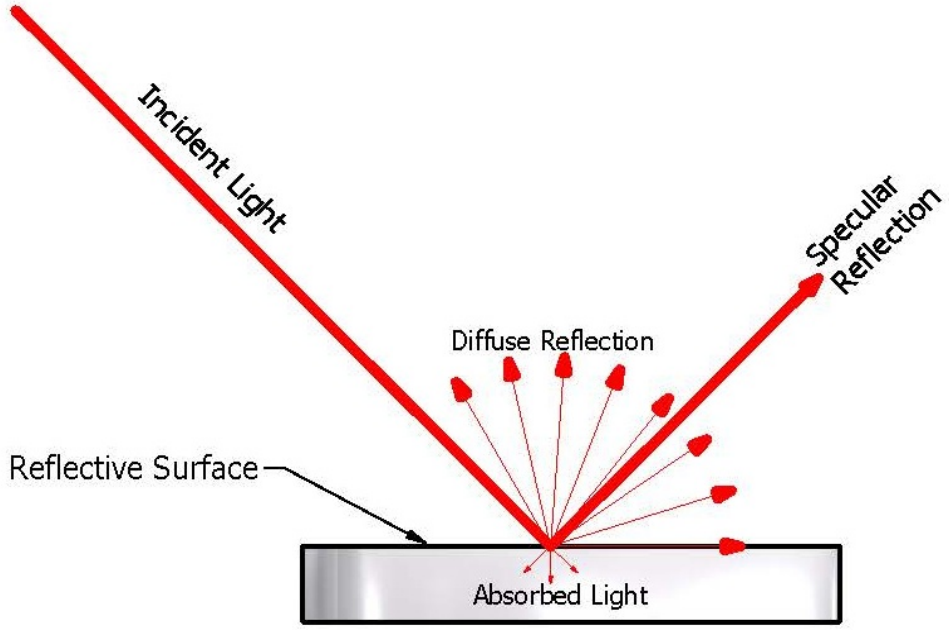

Specular reflectivity is often referred to in literature with other terminology, such as gloss or image clarity. These terms are used to describe surface shininess and the clarity of images reflected from a surface, respectively. The correlation between gloss, image clarity, and specular reflectivity is direct, meaning a lower specular reflectance is equivalent to a decrease in gloss or loss in image clarity.

Measuring Specular Reflectance

Techniques used for measuring specular reflection are often based on a general configuration consisting of a light source, reflective surface, and a detector. The light source generates an incident beam on the reflective surface. The reflected light is then captured with a detector positioned normal to the vector defined by the reflected beam. The position of the light source and detector relative to the reflective surface are arbitrary as long as they reside in the same vertical plane at angles governed by the law of reflection, where the angle of reflection is

equal to the angle of incidence ($\theta_i = \theta_r$) as shown in Figure 1.4.[2,3] The detector measures incident light radiation, which is then converted into an electrical signal and output as a measureable quantity such as power. The result then can be compared to the total power incident on the reflective surface, and produce a relative value used to characterize materials in terms of specular reflectivity. Other typical features of the general system include optical elements to focus the incident beam on the reflected surface, an aperture on the incident beam to prevent any stray light from interfering with the measurement, and an aperture at the entrance of the detector to define the solid angle of the reflected light allowed into the detector. A mathematical representation of the specular reflectance may be defined as:

Equation 1

$$\boldsymbol{\rho_\psi = \frac{1}{I_0}\int_{\psi_1}^{\psi_1+\psi_D}\left(\frac{dI}{d\psi}\right)d\psi, \qquad where\ I_0 = \int_{\psi_1}^{\psi_1+\psi_D}\left(\frac{dI_0}{d\psi}\right)d\psi}$$

where, using the notation similar to that presented by Alexander-Katz and Barrera[4], ρ_ψ is the specular reflectance about solid angle ψ_1, $dI/d\psi$ is the reflected light per solid angle, and ψ_D is the solid angle of light acceptance into the detector as defined by any apertures or receiving optics. The term, I_0 is the total power reflected from a perfectly smooth surface, or in practice a high quality mirror, at an angle θ_r, with $dI_0/d\psi$ equal to the reflected light off the smooth surface per solid angle.

Figure 1.4: Law of Reflection

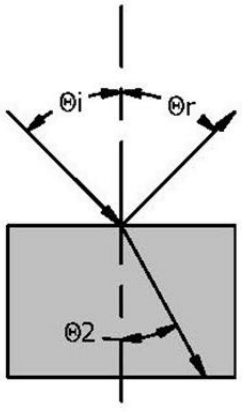

$Law\ of\ Reflection: \theta_i = \theta_r,$

$Snell's\ Law: n_i sin\theta_i = n_2 sin\theta_2$

In a physical sense, relative specular reflection measurements correlate with characteristics of the reflective surface and the incident light. The correlation has been treated mathematically in a model published by Bechmann and Spizzichino[5] for metal surfaces where the characteristic roughness is much less than the wavelength of the incident light. The model, presented in Equation 2, serves to highlight several parameters used to characterize the physical system.

Equation 2

$$\boldsymbol{I = I_0 e^{-\left(\frac{4\pi\sigma cos\theta_i}{\lambda}\right)^2}}$$

From Equation 2, I $[W]$ is the intensity of the reflected light, λ $[nm]$ is the wavelength of the incident light, and θ_i is the incident angle relative to a vector normal to the surface. The remaining variable, σ $[nm]$, is the root-mean-square roughness parameter, which is defined as $\sigma = \sqrt{(h^2)_s}$ where h $[nm]$ is the difference in height between the surface and the mean surface height. The model is based on several assumptions, notably that the surface is an ideal conductor where all of the incident light is reflected, the surface height distribution obeys a normal distribution, and the curvature of the surface is much less than the wavelength of the incident light.[5] The model, under these conditions, is useful for illustrating the relationship between θ_i, λ, and σ. Generally, it may be inferred that the relative specular reflectivity, $\rho_\psi = f(\theta_i, \lambda, \sigma, n_i)$ where n_i, the index of refraction of substance i, has been included for scenarios where the ideal conductor assumption is false.

The Bechmann and Spizzichino model cannot be applied in scenarios, such as an anodized surface, where the ideal conductor assumption is not accurate. When the incident beam contacts a surface for which some fraction ρ is reflected, a fraction α is absorbed and a fraction τ is transmitted according to the relationship shown in Equation 3.

Equation 3

$$\boldsymbol{\rho + \alpha + \tau = 1}$$

The variables in Equation 3 are vector quantities, where the angles of reflected light, θ_r, and transmitted light, θ_2, are governed by the law of reflection and Snell's law as shown in Figure 1.4. With aluminum metal and many of its alloys, the ideal conductor assumption, $\rho \to 1$, is a good approximation[3]; however, this is not the case with the alumina layer, which has been shown to be semi-transparent to light within the visible spectrum.[6] This presents an issue as modeling for light interaction on an anodized surface quickly becomes very complex. As the incident light contacts the anodized surface, some fraction, ρ, is reflected, while the fraction τ continues into the anodic alumina layer refracted at an angle as defined by Snell's Law. The refracted light continues through the layer contacting multiple phases such as pore boundaries, the barrier layer, alloying element imperfections, and metallic grain boundaries amongst others. At each transition, again the light is reflected, absorbed, and transmitted with each material having a different index of refraction and absorption characteristics. The result is a complex interaction that is difficult for a general model to predict.

For the issue being considered by DLC a simplistic approach may be used to provide a relative measurement of specular reflection. DLC is interested in the reduction of specular reflectance, which is described by the specular fraction of ρ. Expanding Equation 3 to include both specular, ρ_ψ, and diffuse, $\rho_{-\psi}$, reflection components results in the following relationship.

Equation 4

$$\boldsymbol{\rho_\psi + \rho_{-\psi} + \alpha + \tau = 1}$$

For DLC, any change resulting in a decrease in ρ_ψ is desirable. While it is expected that in this experiment the bulk of any change will result in a shift from $\rho_\psi \to \rho_{-\psi}$, for the issue in question it is not necessary to distinguish between terms. This leads to a test method where basic comparisons between relative specular reflectivity measurements may be used to evaluate experiment samples.

Anodizing Aluminum

The anodizing process provides a simple method for altering the optical characteristics of the machined aluminum housing surfaces. The process, which found commercial use as early as 1923[3], is well established in industry and has the advantage of being relatively low in cost. In

addition, processing is readily available to DLC through a number of established regional service providers who offer relatively short lead times when using standardized process conditions. The general process, outlined in Table 1, consists of three surface preparation steps, followed by electrochemical growth of a porous anodic alumina layer, and completed by a sealing step[3,7]. The three surface preparation steps, cleaning, etching, and deoxidation/desmut, serve the functions of cleaning, smoothing, and removing loosely adhered metallic compounds from the aluminum surface. These steps serve to prepare a pristine aluminum or aluminum alloy surface for growth of an alumina layer unencumbered by contaminants, oxides, and other compounds that interfere with the layer formation. The layer growth is an electrochemical process in which a current is passed through an electrolyte with a prepared aluminum anode. The current induces the migration of negatively charged O^{2-} anions toward the anode, where they react with aluminum to produce a strongly adherent, robust film over the surface of the anode. Finally, the sealing step serves the function of closing the pore structure of the layer and rendering the film generally inert. In an industrial setting, additional processes such as dye addition, chemical polishing and masking may also be included to achieve specific effects.[3]

Table 1: Industrial Anodization Process Steps

Process Step[3,7,8]	**Step Purpose**
1. Cleaning	Remove contaminants such as lubricants, grease, dust and fingerprints.
2. Etching	Dissolve the aluminum surface to remove embedded impurities and develop a smooth, uniform surface.
3. Deoxidation/Desmut	Remove surface oxides, and loosely adhered metal, metal oxides, and associated compounds.
4. Anodic Alumina Layer Growth	Produce a porous, stable oxide film through electrochemical oxidation of the aluminum surface.
5. Sealing	Close the pore structure of the alumina layer and render the film generally inert.

The structure of the anodic alumina layer, shown schematically in Figure 1.5, consists of an array of hexagonal cells on top of a compact barrier layer. Each cell contains a central pore extending continuously from the external surface of the alumina to the top of the barrier layer, where it terminates with a hemispherical shape. The overall thickness of the alumina layer is dependent on process conditions and may vary from a few microns to several millimeters thick. The continuous barrier layer, typically 10 to 50 nm thick, is positioned immediately above the

aluminum or alloy surface.[9] Above the barrier layer, the close packed hexagonal cells are oriented normal to the substrate surface. For films formed with a sulfuric acid electrolyte, pore and cell diameters are on the order of 10 nm and 30 nm, respectively, although these are strongly influenced by process conditions.[9,10] For pure aluminum substrates the barrier and porous regions are composed of nearly pure alumina, although traces of electrolyte and contaminants are generally present in the structure. This changes for films grown on aluminum alloys where the second phase alloy constituents also become incorporated into the film in partially and completely oxidized states. Depending on the alloy, regularity of the film morphology may be compromised where the non-aluminum phases interact locally with the anodization process causing voids, cracks, film thickness irregularities, and roughening at the alloy-film interface, effecting oxygen migration rates, and altering the chemical solubility of the film.[9,11]

Figure 1.5: Anodic Alumina Layer Schematic

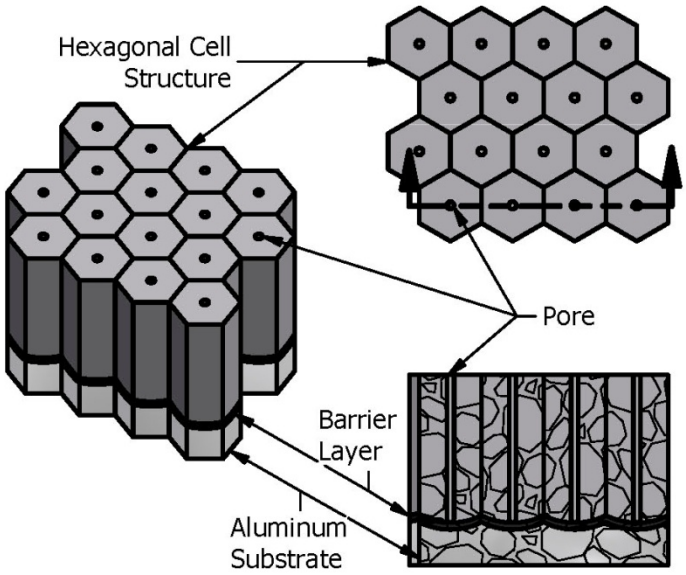

Film growth begins with an electric field assisted oxidation of the aluminum surface with quick formation of a uniform barrier layer of amorphous alumina. As the barrier layer forms there is a continual migration of O^{2-} anions from the electrolyte to the aluminum substrate and a migration of Al^{3+} cations from the substrate to the film surface. Film growth occurs when the O^{2-} anions react with the aluminum substrate, forming new alumina at the film/substrate interface. Outward migrating Al^{3+} cations are ejected directly into the electrolyte creating instability at the film/electrolyte interface. As the barrier layer thickness increases, pores begin

to form at surface locations of locally thinner points or defects in the barrier layer. The pores result in local enhancements of the electric field which also induce greater dissolution of alumina at the electrolyte interface. This process tends to form and stabilize the pore structure, eventually leading to the self-organized, close packed hexagonal cell structure shown schematically in Figure 1.5. Once the pore structure has stabilized, a quasi-steady state is reached, and the process continues with an outward and inward migration of Al^{3+} and O^{2-} ions, respectively, through the base of each pore. The hemispherical shape of the pore base also leads to a scalloping of the substrate surface to maintain a constant barrier layer thickness. New alumina continues to form at the film/substrate interface increasing the overall layer thickness. In theory this process may continue as long as the substrate remains; however, practical limitations exist as the electrolyte also breaks down the alumina at the electrolyte interface, leading to undesirable degradation of the film structure and hardness.[3,8,9]

Anodization Process Variables

Characteristics of the anodic alumina layer are highly dependent on process variables. A review of current literature reveals process variables that affect surface roughness of the oxide film, roughness of the film/substrate interface, optical properties of the film, alumina cell dimensions, film growth rates, film robustness, corrosion resistance, light absorbance, and other characteristics. A summary of the individual variables and their likely effects on the process is included below in Table 2. The first variable is the choice of aluminum purity or one of any number of aluminum alloys.[12] In either case, any non-aluminum, metallic phases present in the substrate interact with the alumina layer formation causing defects and influencing the film structure through both thermodynamic factors and alloying element influence on the general anodization process.[9] In addition, the surface structure of the metal as defined by milling, cutting, rolling, heat treatments, or other processes that create microstructure on the aluminum surface can influence the morphology of the cells structure. For example, recent work on refining the regularity of the cell and pore structure has focused on techniques for creating micro-textured surfaces, which are then used as substrates for anodic alumina film growth.[13,14] The first process step, cleaning, while serving the functional purpose of removing contaminants like oil, grease, detergents and debris, may also affect the aluminum surface. This is particularly true when alkaline and acidic cleaners are used, as these can micro-etch the surface to give

patterned or matte finishes.[3,8] The etch step, by design, removes a thin layer of the aluminum surface to produce a smoothing effect and to remove ground-in impurities. It has also been observed that an alkaline etch process will produce an increasingly matte surface as etch times increase.[3,8,15] The characteristics of the grown alumina layer are controlled by electrolyte, electrolyte concentration, temperature, current density, process potential and time. These variables, both individually and combined, affect the oxide cell diameter, pore volume, film thickness, film growth rates, film density, film hardness, and optical characteristics.[3,6,8,16] Finally, the sealing step, while designed to close the cell pore structure and render the film inert, may also alter the color of the film, giving it a yellow or green hue through changes to film absorbance characteristics.[3,15]

Table 2: Anodization Process Variables

Process Step	Control Variable	Effect
Pre-Process	Metal	The choice of metal, in this case aluminum or one of its alloys, affects the structure and growth of the anodic layer. The alloying elements, present in the aluminum in various forms, influence the porous film growth, film composition and film structure.[8,9,11]
	Metal Surface Preparation	Metal surface appearance generally transfers to the final anodized aluminum surface. For example, mechanical, electrical, and chemically polished surfaces tend to be smoother and more reflective in appearance. Conversely, surfaces roughened or patterned through mechanical means also tend to transfer a matte or patterned appearance to the anodized aluminum surface.[3,8,13-15,17]
Cleaning	Chemistry, Time, Temperature	Alkaline, acid, and solvent cleaners may affect the aluminum surface structure depending on concentrations, time, and temperature. Alkaline solutions may mildly etch the aluminum surface producing a more even, matte finish. Acidic cleaners can give a frosty appearance due to a mild etching of the surface or may provide a chemical polish. The concentration of the materials, time, and temperature of the process control the extent of the effects.[8]
Etching	Etch Rate (NaOH concentration, Temperature) and Etch Time	Alkaline etching of the aluminum tends to smooth and provide a matte appearance to the finished surface. The etching step is typically conducted with a solution comprised of sodium hydroxide, water, and proprietary additives. Concentration, time, and temperature contribute to etch rate and corresponding appearance effects.[3,8,15]
Anodic Alumina Layer Growth	Electrolyte	Many electrolytes are available, with chromic acid, sulfuric acid, oxolic acid, and phosphoric acid all having found commercial uses. The electrolyte used has dramatic effects on the film properties, including color, hardness, film thickness, cell size and others. Of these, sulfuric acid tends to produce films with the smallest cell dimensions, followed by oxolic acid, chromic acid, and phosphoric acid in order of increasing cell size.[3,18]

Process Step	Control Variable	Effect
Anodic Alumina Layer Growth	Electrolyte concentration	Electrolyte concentration directly affects the dissolution rate at the surface of the anodic alumina film. This in turn influences layer thickness and the structural properties of the film. In general terms, higher acid concentrations tend to reduce film thickness and produce softer films.[3,8,16]
	Temperature	Similar in effect to electrolyte concentration, temperature affects the dissolution rate at the surface of the anodic alumina film. Higher temperatures increase the solvent action of the electrolyte leading to softer films and reduced film thickness. Additionally, temperature also may change light absorption characteristics, with lower temperatures producing darker films.[3,6,8,16] Additionally, temperature directly affects the resistance of the electrolyte and anode. For constant current processes, this provides a means of controlling process potential.
	Current Density	Current density is the primary driving force for film formation. Higher current leads to faster film formation and harder, denser films. These films may be darker in color.[3,6,8]
	Potential (voltage)	The forming potential is directly related to process temperature and has a direct effect on cell morphology. Higher potentials produce films with larger cells and larger pores.[3,6,8]
	Time	Time, along with current density, is the primary variable used to control film thickness.[3,8,16]
Sealing	Time, Temperature, Chemical Additives	Sealing the anodic alumina layer with deionized water near its boiling point hydrates the aluminum oxide, increasing its volume and closing the pore structure. The time, temperature and chemical additives (such as nickel acetate) all contribute to the speed and completeness of the process. In addition, the process alters the absorption properties of the alumina film resulting in a greenish or yellowish tint.[3,15]

DLC is most interested in process conditions that are readily available from regional commercial processors, inexpensive to process, and minimize the impact on existing DLC processes. Military specification MIL-A-8625 with Class II, Type I conditions provides a basis to achieve these goals.[7] The specification calls for use of sulfuric acid as the electrolyte in the anodic alumina growth step with no post process dye addition. Per the specification, the process must include cleaning, etching, anodizing, and sealing. The specification also calls for a minimum coating weight of 1000 mg/ft^2. The choice of metal is not specified by MIL-A-8625; however, DLC prefers the use of Aluminum Alloy 6061 with a T6 heat treatment due to its availability, machinability, and cost. Electrolyte concentration has an established industry standard of 15 wt% sulfuric acid in water.[3] Regional service providers typically process materials using a constant current density at an industry standard of approximately 1.29

amps/dm^2 of surface area.[3] Under the conditions listed above and at room temperature, a time of 1 hour is required to meet the coating weight specified by MIL-A-8625.[8] Finally, sealing is necessary to stabilize the film preventing undesirable, or unknown, interactions with DLC technologies for laser and lens attachment.

For the reduction of specular reflectivity, both the etch process variables and factors that affect the morphology of the alumina layer are of interest as both influence the optical properties of anodized aluminum surfaces. More specifically, the etch process has been shown to be influential in the production of low gloss, matte surfaces.[3,8,15,19] This suggests that proper control of the etch process may lead to surfaces with the low specular reflectivity desired for DLC's application. Additionally, alumina layer properties, and specifically morphology of the cell structure, have been cited in previous work to affect gloss, total reflectance, and quality of reflected images off of the anodized surface.[3,6,15] As noted in Table 2, alumina cell and pore dimensions are correlated to the process potential, where increasing the potential increases cell and pore sizes. The process potential is directly related to the resistance in the anodic circuit through Ohm's Law, which may be controlled by process temperature. This allows temperature to be used as a controlling mechanism for the potential and ultimately the cell structure of the alumina layer.

Etching Process Discussion

The etching process, specified by DLC, consists of submerging aluminum alloy parts into an aqueous solution of sodium hydroxide and other additives. The factors influencing this step are the etch rate (a function of temperature and sodium hydroxide concentration) and time. In a commercial setting, it is generally desirable to operate an etch process at elevated temperature and high sodium hydroxide concentration both to increase the etch rate and reduce the overall process time. This leaves the etch time as an attractive control variable for DLC. In practice, the etch time may be correlated directly to etch or aluminum removal rates that may be specified directly with regional commercial service providers.

As stated in Table 2, the purpose of the etch process is to dissolve the aluminum surface to remove embedded impurities and to develop a smooth, uniform base to grow an alumina layer. Functionally, this occurs when aluminum on the surface of the sample combines with sodium hydroxide and water to form aluminate and release hydrogen according to the following reaction:

Reaction 1

$$2Al + 2NaOH + 2H_2O \rightarrow 2NaAlO_2 + 3H_2$$

The reaction proceeds consuming free sodium hydroxide. As the concentration of aluminate increases, a secondary reaction becomes increasingly favorable according to the following formula:

Reaction 2

$$NaAlO_2 + 2H_2O \leftrightarrow Al(OH)_3 \downarrow + NaOH$$

In this reaction, aluminate reacts with water to form aluminum hydroxide, which exists as a suspension in the etch process bath. As shown, the reaction also serves to free up additional sodium hydroxide making it available for Reaction 1. The aluminum hydroxide slowly settles or adheres to various surfaces within the processing tank to form a very hard scale. This occurs according to the following dehydration reaction:

Reaction 3

$$2Al(OH)_3 \rightarrow Al_2O_3 + 3H_2O$$

The resulting net pathway for the etching process is then a reaction between aluminum and water to produce an aluminum oxide precipitate and evolve hydrogen gas.[3,8]

Factors that affect the reaction rates include temperature, sodium hydroxide concentration, aluminum concentration in solution, and the use of additives to discourage aluminum hydroxide scale formation and promote the desirable reactions. For example, Swann and Thomas[20] (as cited by Wernick[3]) reported on etch rates of 99.5% aluminum in an aqueous solution of sodium hydroxide of varying concentrations and temperatures. The results were aluminum removal rates ranging from 0.3 to 5.5 mg/dm^2/min for a temperature range of 30 to 80°C and a sodium hydroxide concentration of 100 g/l. Increasing the sodium hydroxide concentration to 200 g/l over the same temperature range was then reported to yield aluminum etching rates of approximately 0.5 to 7.5 mg/dm^2/min.[3] In addition, as the aluminum concentration in solution increases, free sodium hydroxide is consumed according to Reaction 1.

This effectively lowers the sodium hydroxide concentration until Reaction 2 releases it back into solution. The result is a short term lowering of the aluminum etch rate as aluminum concentration increases past approximately 10 to 20 g/l.[3]

The etching process changes the surface characteristics of the submerged aluminum through a selective removal of aluminum via the pathway described by Beck and Funk.[15] Their recent work investigated the effect of sodium hydroxide etch time on 5005, and 6060 aluminum alloys at 50°C with an average surface removal rate of 1 μm/min. The results indicated an increase in surface roughness, measured as $\Delta R = 5$ μm, after 20 min in the etch bath without further increase through times up to 40 min. The authors correlated this to a ~50% reduction of gloss, an optical property strongly correlated to specular reflectivity. SEM analysis of the etched surfaces revealed the formation of small pits in an even distribution over the sample surface. The pit locations were located at both intermetallic and bulk aluminum phases without an apparent preference for either. However, this was not the case for Staubwasser[21] (as cited by Beck and Funk) who reported preferential etching at AlFeSi and Mg_2Si precipitates.[15] Further investigation in Beck and Funk's work on high purity aluminum suggested that pit formation and corresponding surface roughness tend to occur preferentially at surface sites with higher surface energy crystal facets.[15] In an unrelated investigation, Rao and Raj reported on specular reflectivity changes resulting from an electrolytic etch of ANSI 316 stainless steel designed to mimic corrosion effects. The results, through a fundamentally different etching process, showed a general widening of the exposed grain boundaries, producing an asymptotic decrease in specular reflection in a trend similar to the gloss reduction reported by Beck and Funk.[19] The method for roughness increase and corresponding specular reflection loss of the etched aluminum alloy surface may then be described physically to result from a preferential removal of aluminum and intermetallic compounds at specific surface locations. These locations correspond to grain boundaries, surface defects, intermetallic precipitates and exposed higher surface energy aluminum crystal facets. The result is a roughened surface, on the order of $\Delta R = 5$ μm, having an even distribution over the sample.

Anodization Potential Control and Effect Discussion

The alumina layer growth is an electrochemical process where an electric potential is applied across an anode and cathode submerged in an electrolyte. The resulting current induces a migration of negatively charged O^{2-} anions toward the anode, where they react with aluminum

to produce a strongly adherent, robust film over the surface of the anode. In a constant current process, typically used by DLC's commercial suppliers, the potential is allowed to vary with the changing resistance of the circuit. The resistance is in turn proportional to the process temperature. This allows temperature to be used as a controlling mechanism for the process potential, which has been cited in previous work to be influential in controlling optical characteristics of the alumina film.[6] Most commercial processors available to DLC have temperature control capability since it is necessary to regulate the electrolyte temperature during the slightly exothermic alumina layer growth process. The process temperature, or corresponding voltage, may then be specified directly with regional suppliers to provide DLC's desired, diffuse reflective optical characteristics.

The fundamental effects of anodization potential on the cell structure within the aluminum oxide layer have been characterized by Ono and Masuko[18], who investigated the porosity, pore diameter, and cell diameter of anodic alumina coatings generated on high purity aluminum in 1.5 mol/dm^3 sulfuric acid and other electrolytes. TEM measurements of the cell diameter and measurements of porosity using a technique called re-anodizing are documented elsewhere.[18,22,23] Pore diameter was then determined according to the following relationship:

Equation 5

$$\alpha = \left({}^{d_{pore}}\!/\!_{d_{cell}} \right)^2$$

where α, d_{pore}, and d_{cell} refer to porosity, pore diameter and cell diameter, respectively. Some results of the work are shown below in Figure 1.6 for the anodization process conducted in sulfuric acid with a potential range of 10 to 20 volts.

Figure 1.6: Pore Dimensions[18]

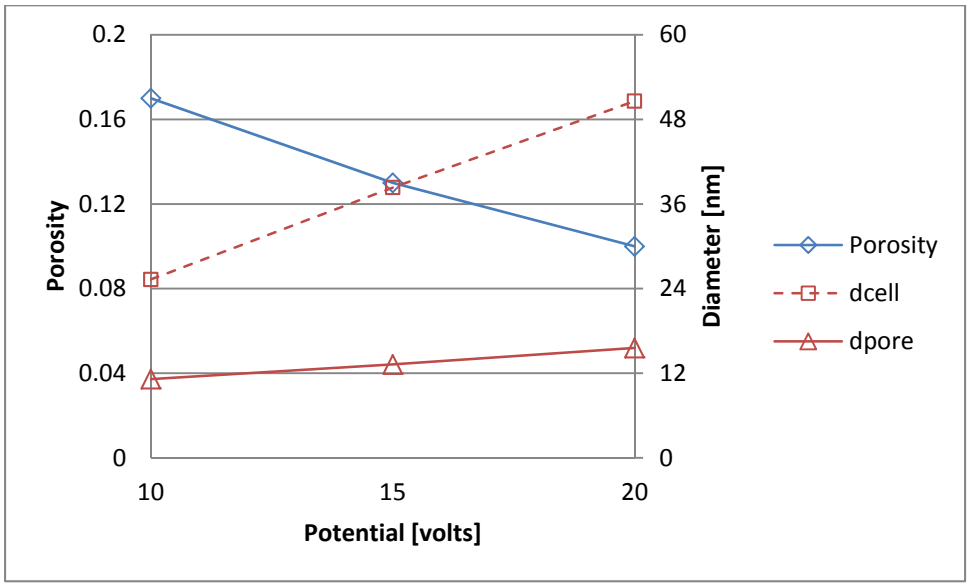

Ono and Masuki's findings show a decrease in porosity and an increase in both cell and pore diameters over a potential range of 10 to 20 volts. The cell wall thickness, which can be estimated by $d_{cell} - d_{pore}$, also increases with potential.

For a constant current process, the shape of the potential versus time curve is indicative of the anodic alumina layer formation and growth. As shown in Figure 1.7, at the initiation of the process there is a rapid increase in potential, which coincides with barrier layer formation and rapid thickness increase.[6] After which, pores form at the barrier layer surface, gradually increase in size, and then self-arrange. This occurs until a quasi-steady state is reached as indicated by the potential becoming relatively constant over short, 3 to 5 minute time ranges. As this is a constant current process, Ohm's Law dictates that the resistance must change to control the potential. This is most easily accomplished by changing the anodization electrolyte temperature, although it has also been shown that a similar effect may be achieved by controlling the anode temperature directly.[16]

Figure 1.7: Characteristic Potential Curve

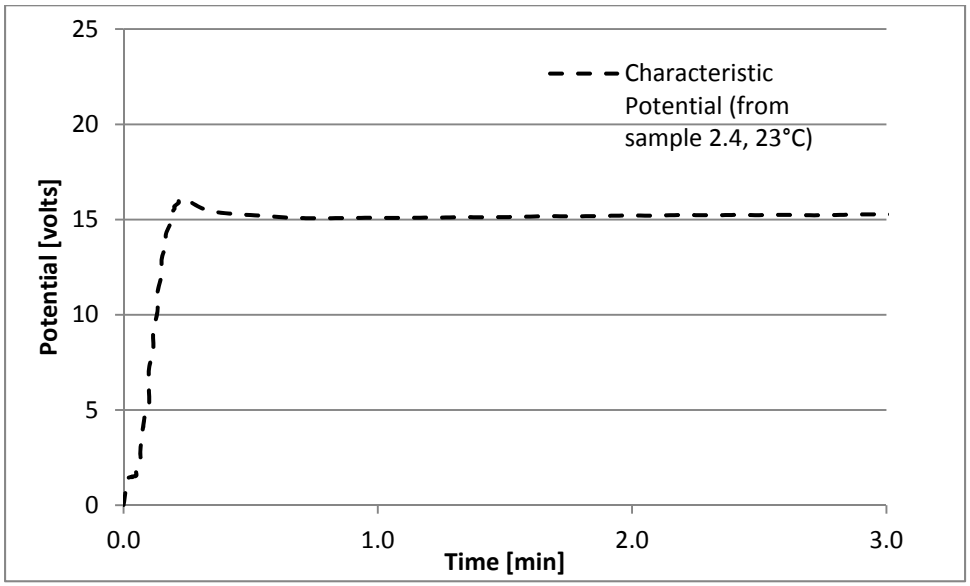

While potential is the primary control variable for cell morphology, inducing potential changes with temperature has a minor effect on other cell structure characteristics. Shih, Wei and Huang[6] demonstrated that a temperature increase of 10 to 30°C results in a small decrease in the porous film thickness. In their study, the decrease was on the order of ±5%, with 15 wt% sulfuric acid and a current density of 1.5 amp/dm^2 on Al1050. This is a result of an increase in electrolyte attack on the film surface.

The effects of cell morphology on the optical characteristics of the anodized film are more difficult to quantify. Early investigations, published by Cochran and Keller[24] (as cited by Wernick[3]) show a degradation of reflected image clarity with increased process potential resulting from lowering the process temperature. Their work, conducted on hardened 5357-H25 Al-1.0% and 5557-0 alloys, also indicated markedly different image clarity versus potential curves depending on which alloy was used. More recently, Beck and Funk[15] studied the effect of anodic oxidation on gloss with 5005 and 6060 aluminum alloys. Their experiments, which used a 2M sulfuric acid electrolyte at 20°C and operated at 18 volts, revealed a ~17% decrease in measured gloss. Since surface roughness changes were negligible, their investigation concluded that the partially transparent alumina layer chemical and structural properties were responsible for the decrease. A third example was shown in a recent work by Shih and Wei[6] who investigated the optical properties of aluminum oxide generation on Al1050 alloys. Their work

investigated total reflectivity as a function of potential, current, and anodization temperature, which were used to control the alumina layer structural properties including pore density and film thickness.

Chapter 2 - Experimental Design

Experiment Design Space

To explore the effect of the etch time and anodization potential on the specular reflectivity of an anodized 6061-T6 aluminum surface, a central composite experimental design structure was used. The design space, shown schematically in Figure 2.1, consisted of two control factors: etch process time and anodization process temperature. The process temperature is directly proportional to anodization potential under similar conditions.[6,16] Three trials were conducted at the center point to provide an estimate of repeatability. The total experiment then consisted of eleven total trials including nine design points and two repeat trials at the central condition.

Figure 2.1: Experiment Design: Specular Reflectivity vs. Etch Time [min] and Anodization Temperature [°C]

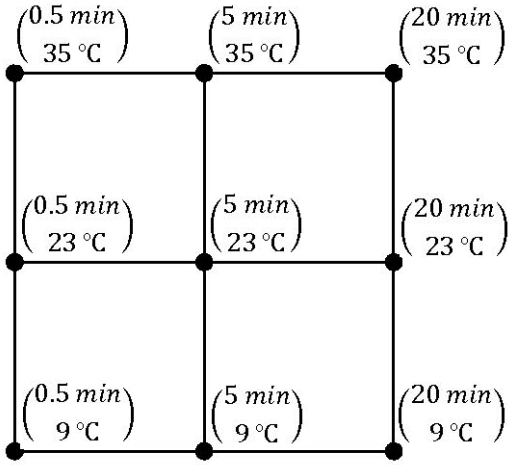

The range of etch times were chosen based on results obtained in studies by both Beck and Funk[15] and Rao and Raj[19]. In Beck and Funk's work, 5005 aluminum alloy in a sodium hydroxide etch process at 50°C resulted in the relationship shown in Figure 2.2 where a steady-state roughness was reached after approximately 20 minutes in the process bath.[15] Similarly, Rao and Raj[19] reported an asymtoptic decrease in the specular reflectivity of stainless steel due to a etch process time. For this experiment, sample points of 0.5, 5, and 20 minutes were selected to capture a point where the etch process had minimal effect on specular reflectivity, a point

where specular reflectivity was in a rapid state of change, and at a point where the specular reflectivity as a function of etch time had stabilized.

Figure 2.2: Roughness vs. Etch Time[15]

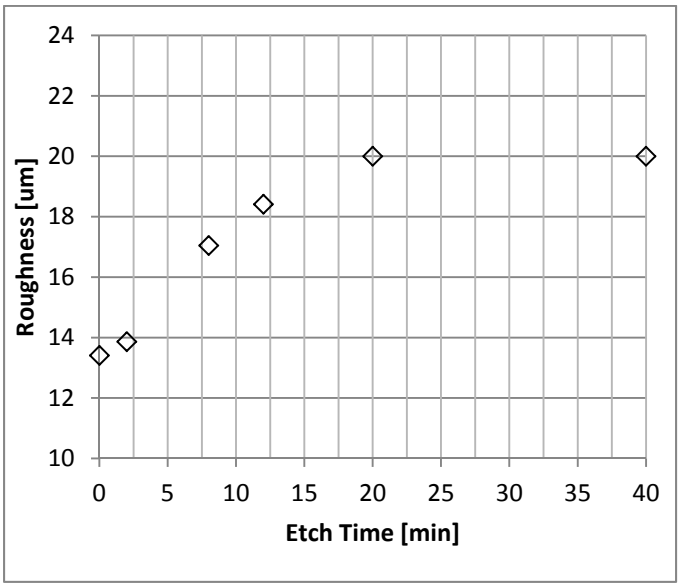

The anodization process temperatures were chosen based on work conducted by Shih et al[6]. Their work demonstrated a ±5 volt potential shift by raising the process bath temperature ±10°C in a 15 wt% sulfuric acid electrolyte controlled to 1.5 amps/dm^2. Temperature factor conditions of 9, 23, and 35°C for the anodization bath were then selected to provide a similar ±5 volt shift in the characteristic potential curve and to operate at setpoints easily maintained by the experimental setup.

Process

For the experimental runs, a small pilot anodizing system was constructed in a manner consistent with standard commercially available processes. The system consisted of five polypropylene process tanks, one for each step outline in Table 1. Each tank contained 6 L of fluid and was insulated for improved thermal stability. Agitation was provided by pumps bubbling air through perforated tubes mounted in the base of each tank. The cleaning, etching, and sealing tanks were also fit with thermostat-controlled, submergible, 500W stainless steel heating units. For the anodizing tank, heating and cooling were provided by means of a submerged coil through which temperature regulated water was pumped to produce the desired

electrolyte temperature. The current for the process was supplied by means of an Agilent E3644A, 80W power supply set to provide 1.29 amps/dm^2. The process potential was allowed to vary, while being monitored, to maintain a constant DC current. Potential measurements in the anodizing process were made via a Fluke 189 Multimeter sampling once per second.

As with the physical setup, the experiment's process conditions were set to be consistent with commercial processes. A summary of these conditions is presented in Table 3. The cleaning process included a 5 minute soak in an agitated, mild alkaline bath heated to 60°C. The cleaning bath contained additives and was diluted per manufacturer specifications to prevent etching. Next, the samples were removed and thoroughly rinsed with distilled water before being placed in an agitated sodium hydroxide etch bath. The etch bath was regulated at a temperature of 60°C, while the etch time varied per experimental test condition. Once the etch time expired, the samples were thoroughly rinsed and then were placed in the deoxidation/desmut bath for 60 seconds at room temperature. After another thorough rinse, the samples were then placed in the 15 wt% sulfuric acid tank, preconditioned to an appropriate temperature per test condition, for anodizing. For consistency, the samples were placed in the center of the anodization tank and oriented approximately 10 cm directly across from a 6061-T6 aluminum cathode. The anodizing process was followed by a thorough rinse and a 20 minute sealing process in an 82°C nickel acetate bath. The ingredients for the cleaning, etch, deoxidation/desmut and sealing steps were provided by US Specialty Color Corporation® and employed at conditions consistent with recommended use. The sulfuric acid for the anodization process was supplied by East Penn Manufacturing Co., Inc. and diluted to the correct ratio with distilled water.

Table 3: Anodizing Process Conditions

Process Step	Process Conditions
1. Cleaning	• Time: 5 minutes • Temperature: 60°C • Chemistry: 74.9 g/l Specialty 740 alkaline cleaner in distilled water. Cleaner was provided by US Specialty Color Corporation®
2. Etching	• Time: Variable (0.5, 5, & 20 min) • Temperature: 60°C • Chemistry: 44.9 g/l Specialty 835 alkaline etch in distilled water. Etch was provided by US Specialty Color Corporation® • Active Ingredient: 36.0 g/l NaOH • Other Ingredients: Proprietary scale inhibitors
3. Deoxidation/Desmut	• Time: 1 minutes • Temperature: 23°C • Chemistry: 171.6 g/l (12% vol.) Specialty 982 Deoxidizer in distilled water. Deoxidizer was provided by US Specialty Color Corporation® • Active Ingredient: 27.5 g/l sulfuric acid • Other Ingredients: Proprietary additives
4. Anodic Alumina Layer Growth	• Time: 60 minutes • Temperature: Variable (9, 23, & 35°C) • Chemistry: 15 wt% sulfuric acid in distilled water. Sulfuric acid was provided by East Penn Manufacturing Co., Inc. • Active Ingredient: 45.76 g/l sulfuric acid • Other Ingredients: None
5. Sealing	• Time: 20 minutes • Temperature: 82°C • Chemistry: 3% vol. Specialty Sealant MTL nickel acetate sealer in distilled water. Sealer was provided by US Specialty Color Corporation® • Active Ingredient: 0.12 wt% nickel acetate • Other Ingredients: Proprietary additives

Sample Preparation

Samples were prepared to render a clean, flat, uniform surface for measuring the specular reflection. The intent was to provide a surface polish exceeding what could be expected from a machinist supplying components to DLC. As an additional requirement, a flat test surface was necessary as any curvature would cause a shift in the reflected beam, skewing the specular reflectivity measurements.

Each sample consisted of a 24 mm long test cylinder with one end prepared for specular reflectance testing. All samples were cut from a single 9.5 mm diameter rod of 6061-T6 aluminum. The composition for this alloy is shown below in Table 4. For the test surfaces, each cylinder was milled flat on one end by cross-cutting with an endmill. Next, the cross cut machining marks were removed using a fine-grain ball mill grinding in a spiral pattern with a 0.1 mm constant pitch. Finally, the test surfaces were hand buffed to a near mirror finish. All samples were cleaned with acetone in an ultrasonic bath prior to use.

Table 4: 6061 Aluminum Composition

Composition Element	Al	Si	Cu	Mg	Cr
Weight %	97.9	0.60	0.28	1.0	0.20

Test Method

The test setup is based on a concept presented by Peiponen, Myllyla, and Priezzhev[2] for online measurement of moving sheet materials and is shown schematically in Figure 2.3. For the laser source, DLC constructed a custom module consisting of a laser diode, focusing lens, aperture, and an electronic driver circuit. The laser diode emits a coherent beam at a wavelength of 660 nm. Using feedback from an integrated photodiode, the laser diode operates on a control loop to provide a constant output power, I_0, of 45.9 mW. The circuit is capable of achieving virtually constant power over moderate temperature changes, which may be achieved at room temperature with adequate heat sinking. The focusing lens is positioned to provide a collimated incident beam aimed at the center of the reflective sample. A small aperture is positioned immediately after the focusing lens to prevent stray light artifacts from influencing the measurement. A commercially-available Thorlabs S142C Integrating Sphere with a built-in 12 mm aperture is employed for the detector. The integrating sphere is connected to a Thorlabs PM100D power meter providing a measurement signal in milliwats.

This experiment utilized two test methods to provide relative measurements between experiment samples. In the first method, the laser source was fixed at location 15.9 mm away from the sample, and the relative angle between the laser source and the detector was fixed at $\theta = 45°$. The detector was positioned normal to the reflected beam, as shown in Figure 2.3. Since

the detector has an integrated 12 mm aperture, the detector position was varied to change the acceptance angle of incident light. Detector positions A, B, and C, then corresponded to light acceptance angles of 13.1, 6.6, and 3.8°, respectively. The second test was designed to provide information on the angular dependence of the specular reflection. The test uses the same experimental setup, except that the detector and source distances from the sample were fixed at 15.9 mm and 63.0 mm, respectively, resulting in an acceptance angle of 8.7°. The test was then conducted by changing the angle, θ, from 15° to 52.5° while monitoring the effect on specular reflection.

Figure 2.3: Test Setup

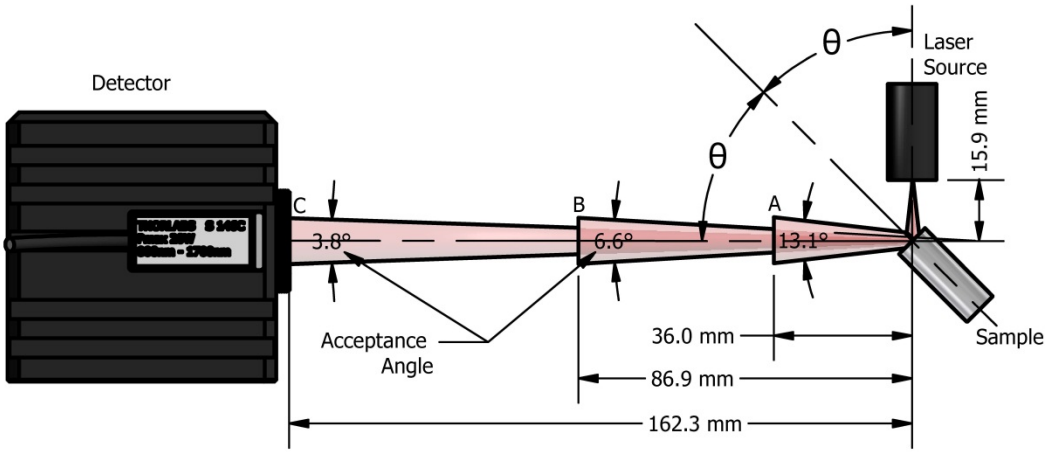

Chapter 3 - Results

Anodization Characteristic Potential Response to Temperature

The effect of the electrolyte temperature on the characteristic potential for the anodization process step is shown in Figures 3.1 and 3.2. The plots display the measured potential as a function of time for the process conducted with a constant current flux of 1.29 amps/dm^2 for the initial 3 minutes and 1 hour in Figures 3.1 and 3.2, respectively. The three curves correspond to electrolyte temperatures of 9, 23, and 35°C. All three curves are characterized by a rapid initial increase in potential that is a consequence of the barrier layer formation within the first 8 to 11 seconds of the process. Next, as the nanopores begin to form, widen, and self-arrange, the potential peaks and then undergoes a decrease before reaching a quasi-steady state condition. As shown, this effect is more pronounced for processes conducted at lower temperatures. The evolution of the potential curves recorded during this experiment show good agreement with previous results.[6, 16]

Figure 3.1: Process Potential (3 minutes)

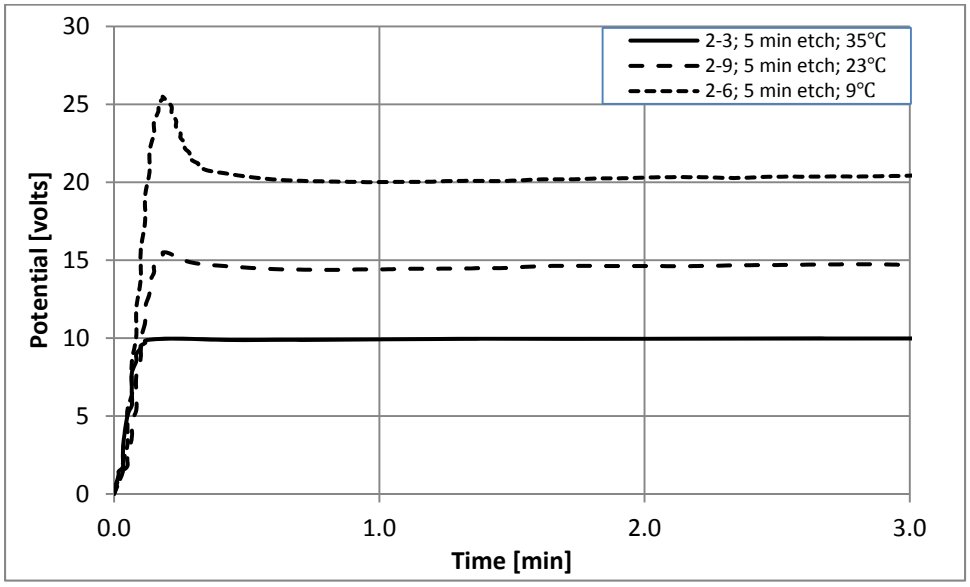

Figure 3.2: Process Potential (1 hour)

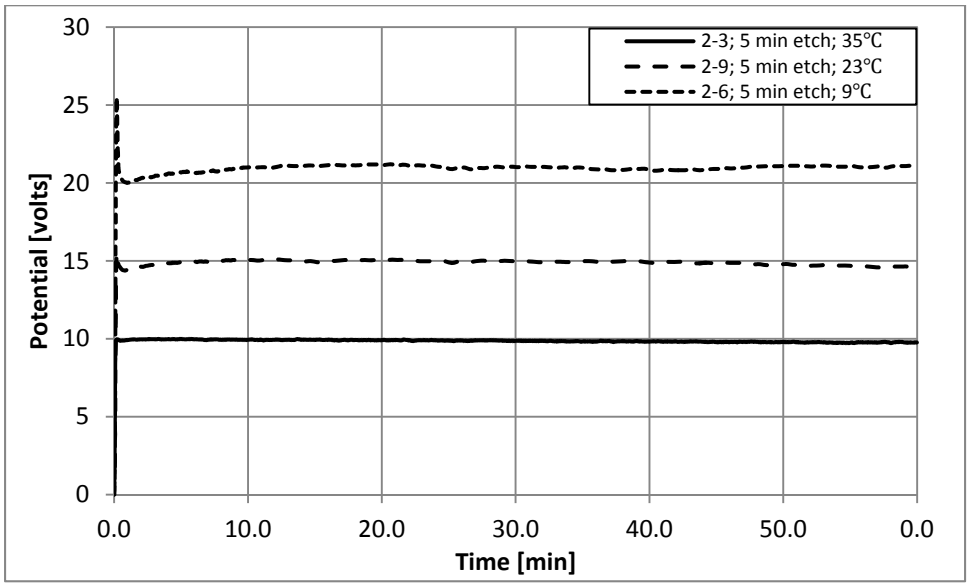

The relationship between potential and temperature is shown in Figure 3.3 over the temperature range from 9 to 35°C. For a process operating at 1.29 amps/dm^2, the measured quasi-steady state potentials are 9.9, 15.1, and 20.9 volts at 9, 23, and 35°C, respectively. Fitting the data points to a linear model results in a slope corresponding to a 0.42 volt/°C potential decrease over the experimental conditions. Clearly, the difference between the quasi-steady state potential and the peak potential increases as the temperature decreases. The peak potentials observed were 9.9, 15.5, and 25.4 volts at 9, 23, and 35°C, respectively.

Specular Reflectance

The specular reflectance was measured on samples prepared at each of the design conditions shown in Figure 2.1 using the test setup described in Chapter 2 with an incident angle of $\theta = 45°$. The results were plotted as a function of acceptance angle and reported as a percentage of the total incident power on the sample, I_0=45.9 mW. Where applicable, the results were presented as a function of the quasi-steady state anodization potential, which was directly related to the electrolyte temperature in the anodizaton process according to the relationship presented in Figure 3.3. Photographs of the optical images reflected onto a target 300 mm from the sample surface were also recorded in the following figures to provide a visual comparison of the results.

Figure 3.3: Potential vs. Temperature Relationship

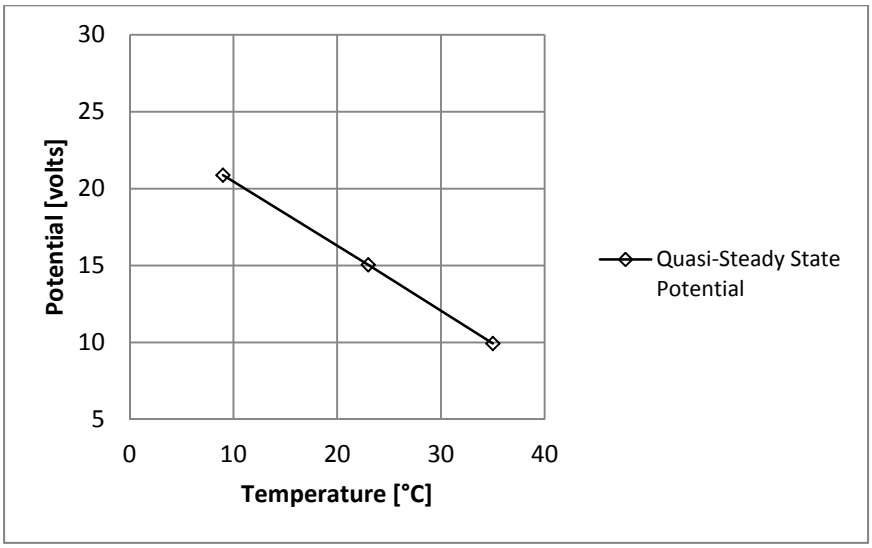

Baseline Specular Reflectance

To provide a baseline for comparison, additional specular reflectance measurements were recorded for a mirror and three non-anodized, polished aluminum samples. For the measurements, the non-anodized samples and mirror were substituted in place of the sample shown in Figure 2.3. The mirror yielded a nearly constant specular reflectivity of 96.9% as shown in Figure 3.4. This coincided with a reflected optical image, shown in Figure 3.5, which largely retained a collimated intensity profile much smaller than the acceptance aperture of the detector. Also evident in Figure 3.5 was a low level of scattered light outside of the central beam that accounted for the 3.1% loss in the specular reflectivity measurement. The three non-anodized samples were prepared according to the method described Chapter 2 and were hand polished with the intent of exceeding the typical finish DLC has received on machined aluminum components. As shown in the second photograph presented in Figure 3.5, the reflection from a representative polished surface results in an image with a pronounced central spot surrounded by a pattern characteristic of diffuse reflection. This is also indicated in Figure 3.4, where the specular reflectance measurements show a decrease from the mirror value of 96.9% to between 61% and 75%.

Figure 3.4: Specular Reflectivity of Polished Surfaces

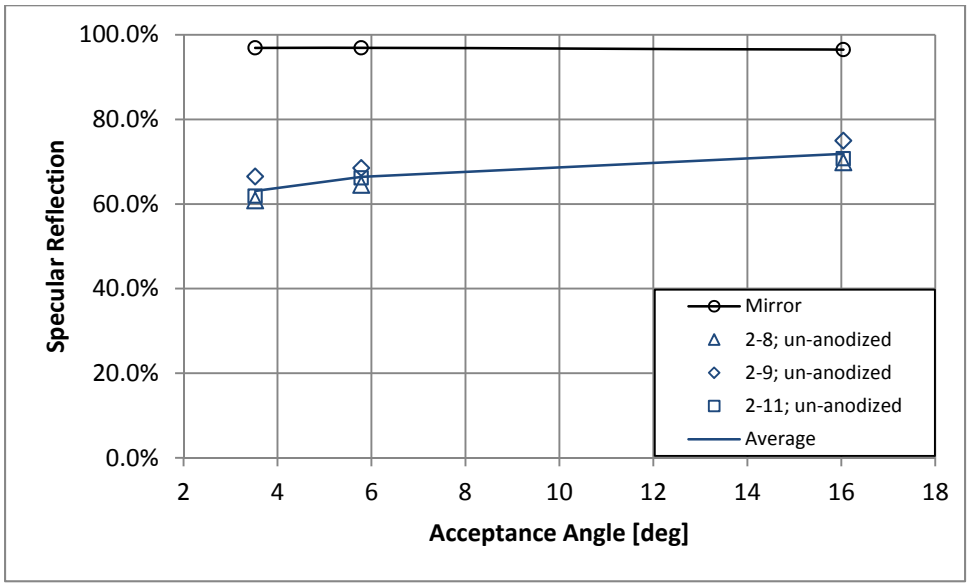

Figure 3.5: Mirror and Polished Sample Optical Image

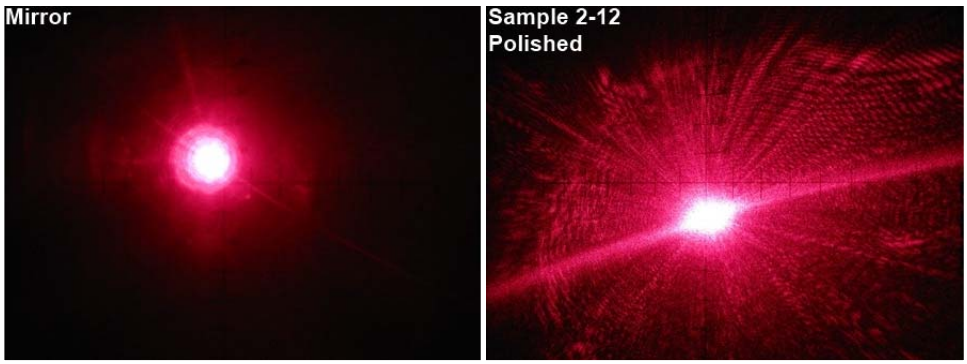

Center Point Agreement

To provide an estimate of process repeatability, three identical trials were conducted at the centerpoint of the experimental design space. The three samples, used to provide the baseline measurement shown in Figure 3.4, were processed with a 5 minute etch time and a 23℃ electrolyte bath, corresponding to a 15 volt quasi-steady state process potential. The samples were tested for specular reflectivity with the results shown as a function of acceptance angle in Figure 3.6. Optical images were also presented for a visual comparison in Figure 3.7.

The specular reflectance measured on the three samples may be used as a rough estimate of sample-to-sample repeatability to compare with further results. As shown in Figure 3.6, the range between the three sample measurements are 0.06, 0.16, and 0.76% for acceptance angles

of 3.8, 6.6, and 13.1°, respectively. The projected images for each sample are shown in the photographs displayed in Figure 3.7. These demonstrate that the three samples are virtually undistinguishable.

Figure 3.6: Center Point Repeatability

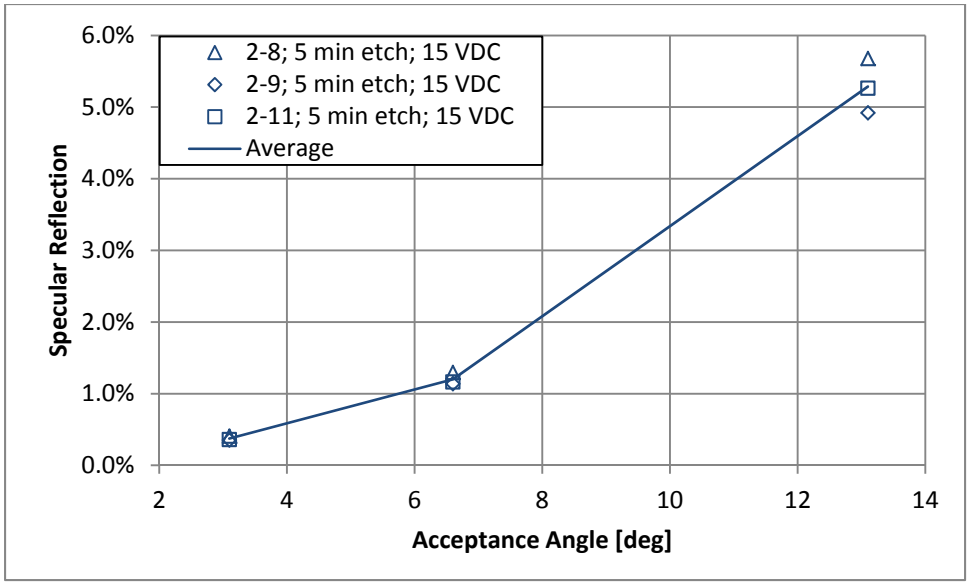

Figure 3.7: Optical Images; Centerpoint, 5 min etch, 15 volts

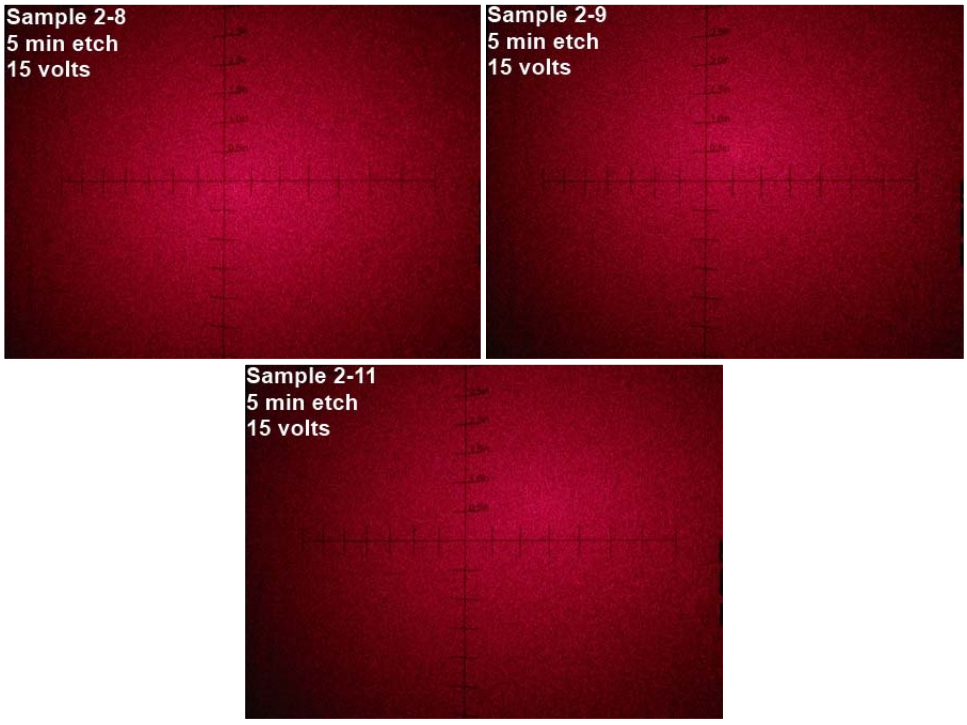

Specular Reflectance vs. Etch Time

The effect of etch process time may be seen by comparing Figures 3.8, 3.10 and 3.12. The general trend is a decrease in specular reflectivity with increasing etch time. This trend is consistent for all of the tested acceptance angles, but is most clearly seen with the measurements at 13.1°. These have been summarized in Figure 4.1. At this acceptance angle, the measured specular reflectance ranges from 7.3% to 20.6% for a 0.5 minute etch process (Figure 3.12). The values decrease for the samples with 5 and 20 minutes etch processes, resulting in ranges of 2.4% to 5.3% and 1.2% to 2.3%, respectively.

The effect of etch process time is also evident in a visual analysis of the captured images shown in Figures 3.9, 3.11, and 3.13. For samples produced with a 20 minute etch time, the reflection images shown in Figure 3.9 display a diffuse, dim intensity profile with no distinguishable central spot. The images captured in Figure 3.11, reflected from samples produced with a 5 minute etch time, are noticeably brighter, yet still diffuse without a central spot. In contrast, the images presented in Figure 3.13, reflected from samples with a 0.5 minute etch process, are bright with a clearly defined central spot. Additionally, images from the 15 and 21 volt samples show a light band crossing the photo similar in shape to the band crossing the polished sample reflection shown in Figure 3.5.

Figure 3.8: Specular Reflection, θ = 45°, 20 min Etch

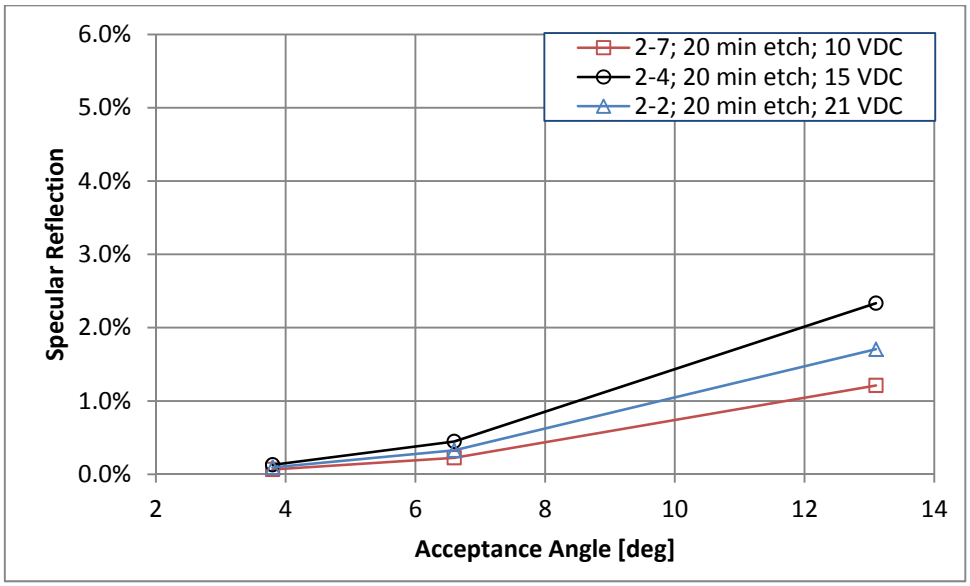

Figure 3.9: Optical Images, 20 min Etch

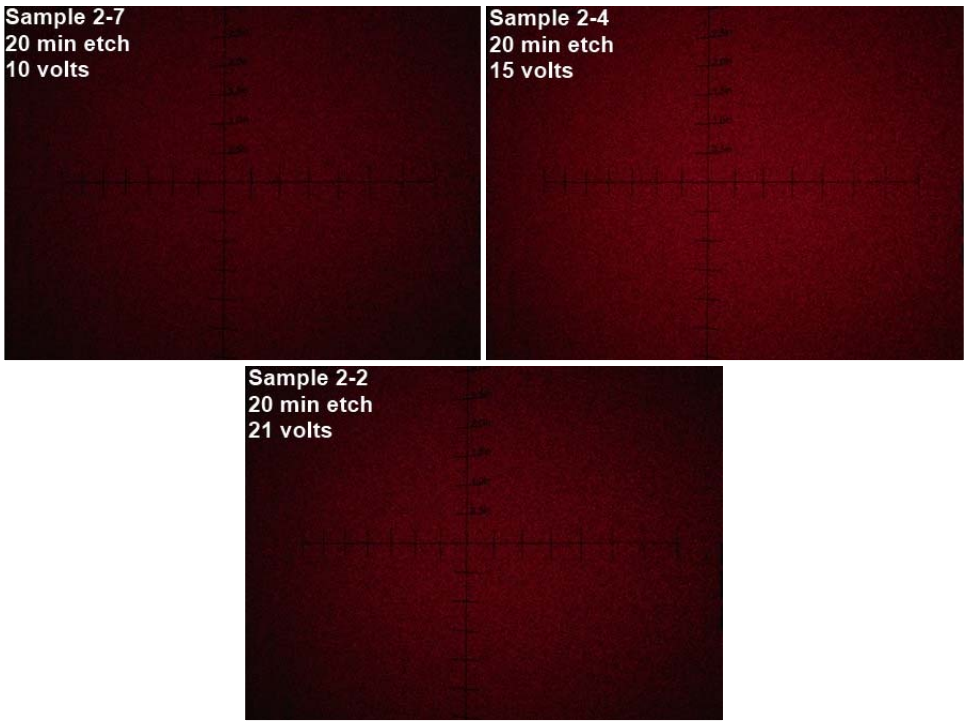

Figure 3.10: Specular Reflection, θ = 45°, 5 min Etch

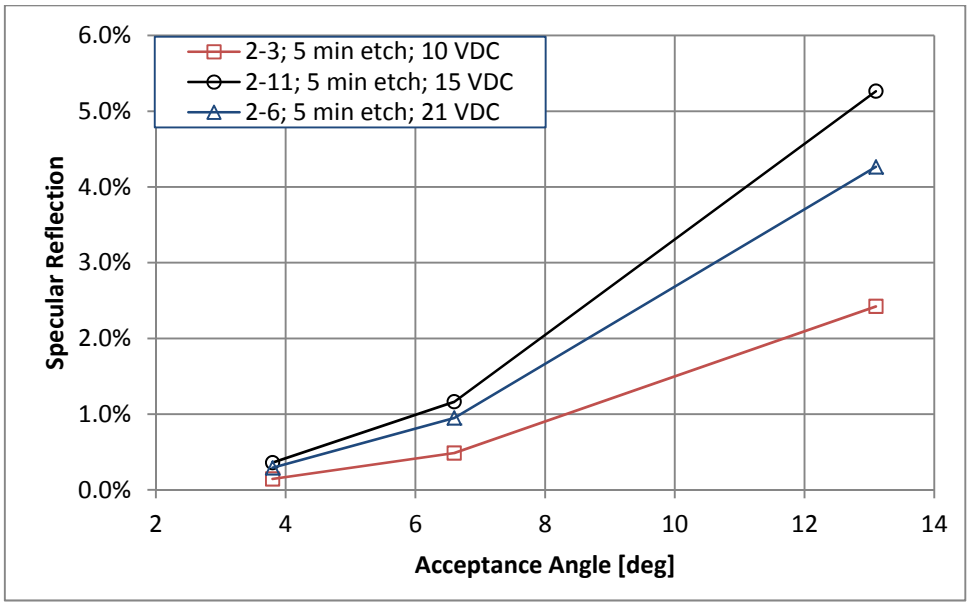

Figure 3.11: Optical Images, 5 min Etch

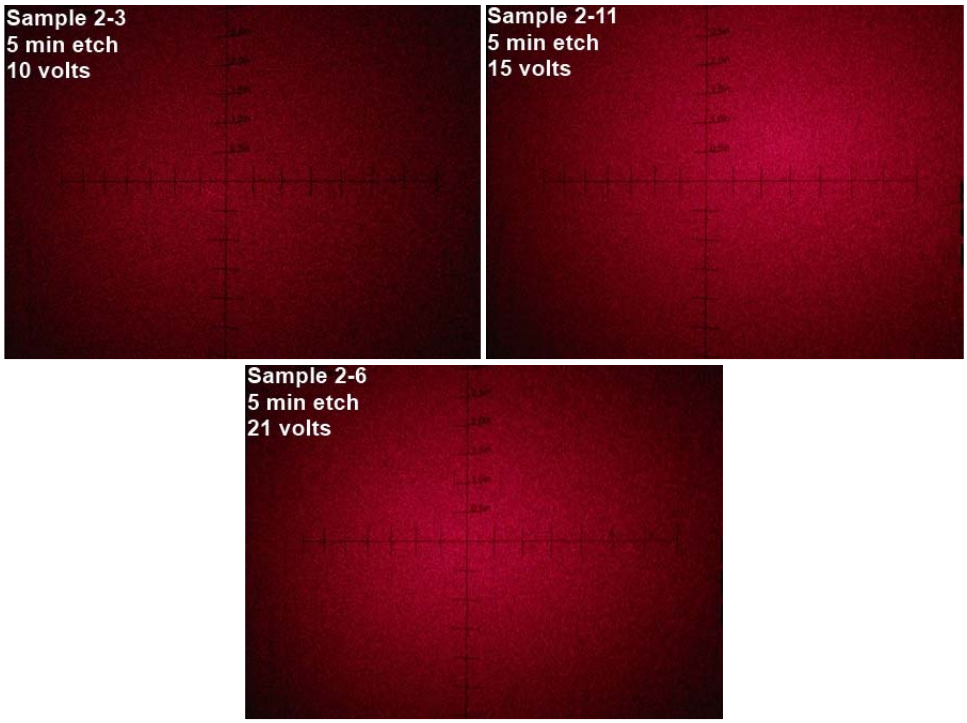

Figure 3.12: Specular Reflection, θ = 45°, 0.5 min Etch

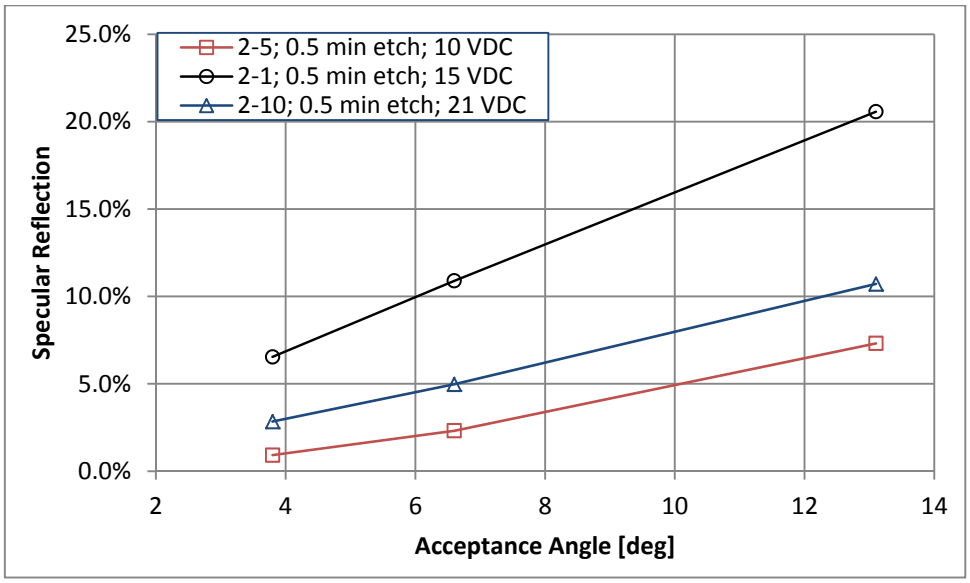

Figure 3.13: Optical Images, 0.5 min Etch

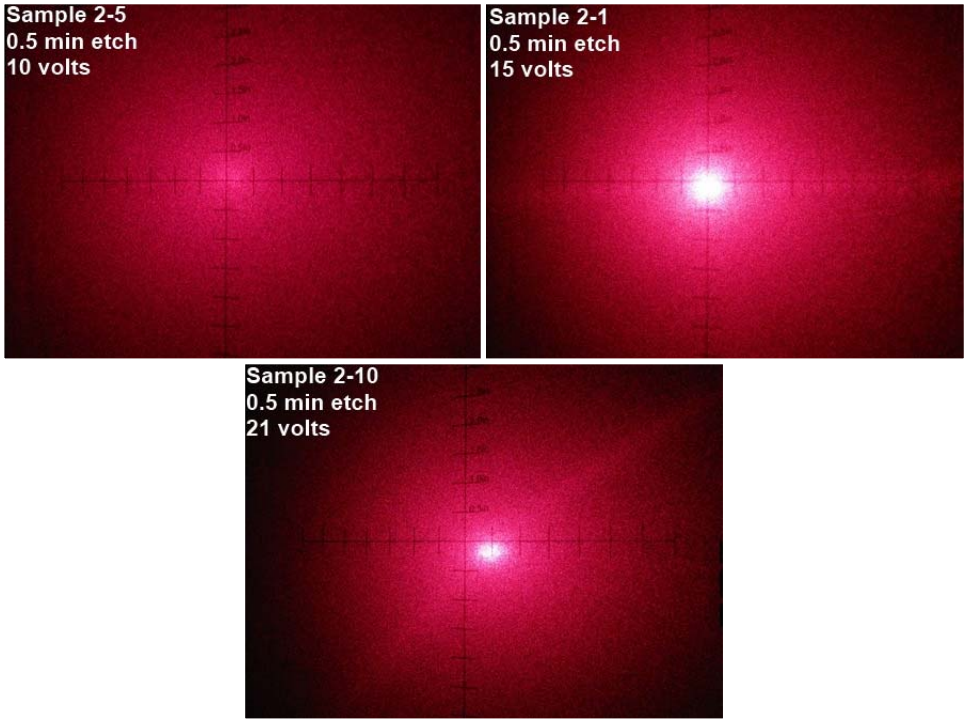

Specular Reflectance vs. Anodization Potential

The effect of anodization potential on specular reflectance was consistent. For a given etch process time, the samples produced at a 15 volt quasi-steady state potential produced the highest specular reflectance. Increasing or decreasing the potential lowered the specular reflectance, with the 10 volt condition producing the lowest values. This trend is summarized Figures 3.14 and 3.15 for sample measurements recorded with an acceptance angle of 13.1°. Error bars showing the 0.76% range measured during the center point repeatability testing are superimposed on the test points for comparison. As shown in Figure 3.14, the difference between specular reflectance measurements from the three samples etched for 20 minutes are small. The difference between measurements is more pronounced with the samples etched for 5 minutes and more clearly show that the sample anodized at 15 volts has the highest specular reflectance. Figure 3.15 displays the same pattern for samples etched for 0.5 minutes where again the highest specular reflectance is measured on the sample anodized at 15 volts. The trend is also visible in the images presented in Figures 3.9, 3.11, and 3.13. The reflections from samples etched for 20 minutes, shown in Figure 3.9, are largely similar in appearance although the 10 volt condition has a slightly lower intensity. The same is shown in Figure 3.11 for samples produced with a 5 minute etch, where the 10 volt condition has a lower intensity. In the third set of images, Figure 3.13, the differences in reflection profiles are visible with the reflection from the 15 volt sample showing a bright central spot. The central spot diminishes and nearly disappears in the samples produced with 21 and 10 volt potentials, respectively.

Figure 3.14: Specular Reflection (5 and 20 min Etch)

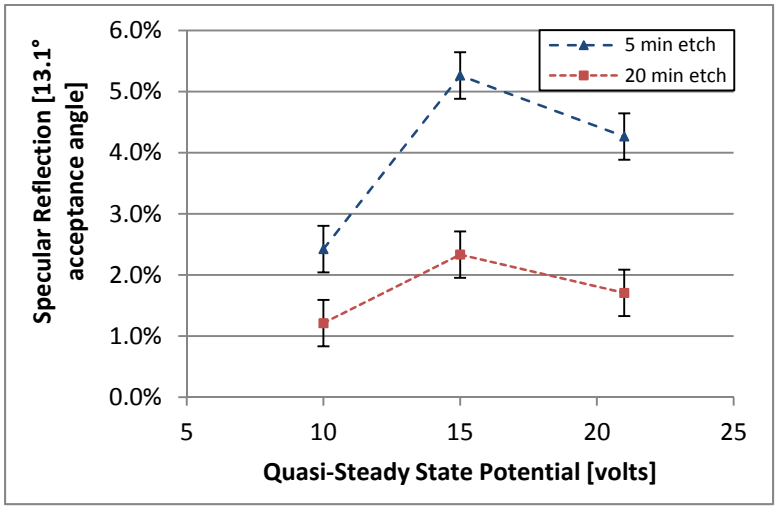

Figure 3.15: Specular Reflection (0.5 min Etch)

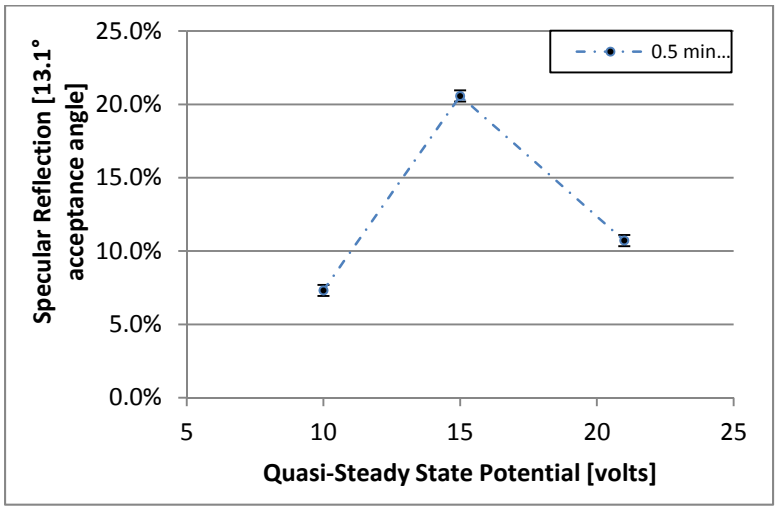

Angular Dependence of Specular Reflectivity

Further testing was conducted on the samples to investigate the angular dependence of the incident beam angle on the specular reflectivity measurements. These measurements were of interest since the Bechmann and Spizzichino model, shown previously in Equation 2, suggested that the specular reflection, I/I_o, was a function of θ_i (the incident beam angle relative to a vector normal to the surface)[5]. The test was conducted by fixing the distance of the laser source and detector, positioned as shown in Figure 2.3, at 15.9 mm and 63.0 mm, respectively. This setup resulted in an acceptance angle of 8.7° for the detector. Measurements were then recorded while varying θ from 15° to 52.5° in 7.5° increments. The results are displayed in Figures 3.16 through 3.19.

The three center point samples were again analyzed to show a range for sample-to-sample variances. As shown in Figure 3.16, the three samples produced a similar trend in specular reflectance as the incident angle increased from 15° to 52.5°. The range between measurements at each incident angle varied between 0.22 and 0.33%. Where appropriate, error bars reflecting these ranges have been added to Figures 3.17 through 3.19 to provide an estimate of the sample-to-sample variance.

Figure 3.16: Center Point Angular Dependence

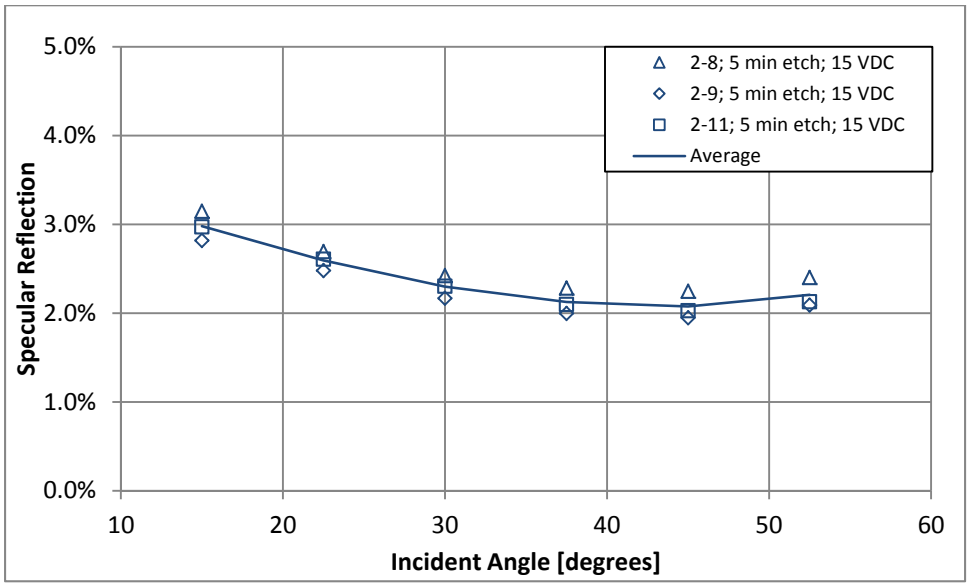

Figure 3.17: Specular Reflection, Variable θ, 20 min Etch

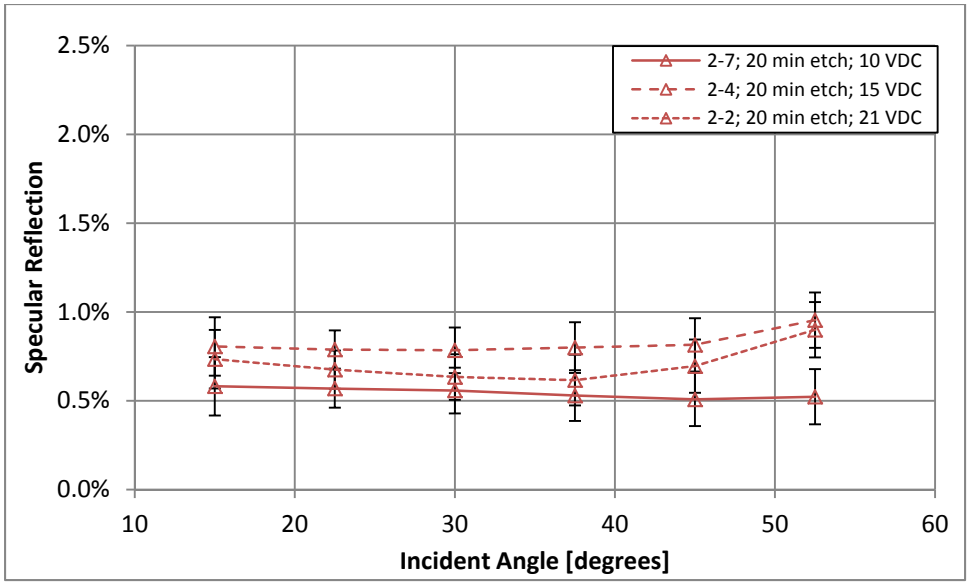

Figure 3.18: Specular Reflection, Variable θ, 5 min Etch

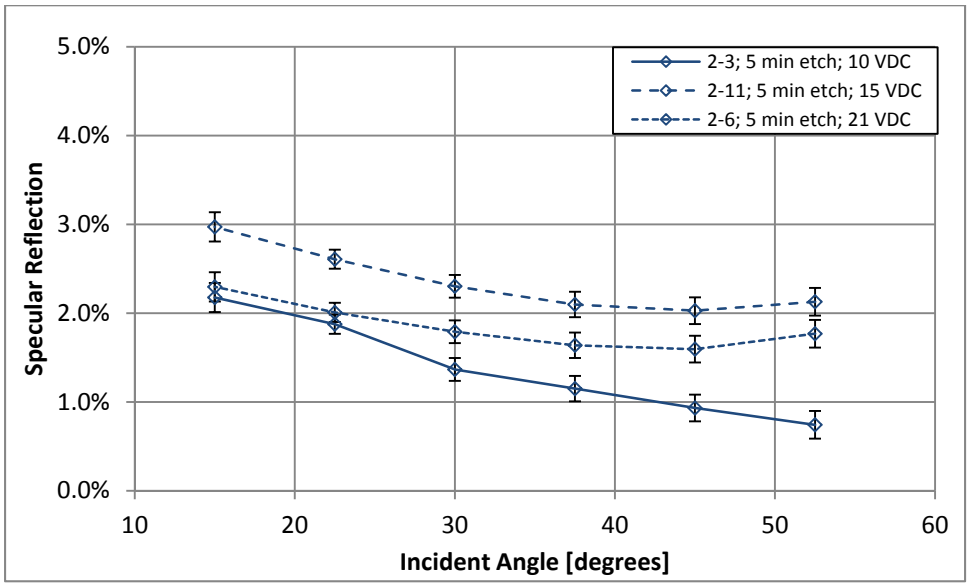

Figure 3.19: Specular Reflection, Variable θ, 0.5 min Etch

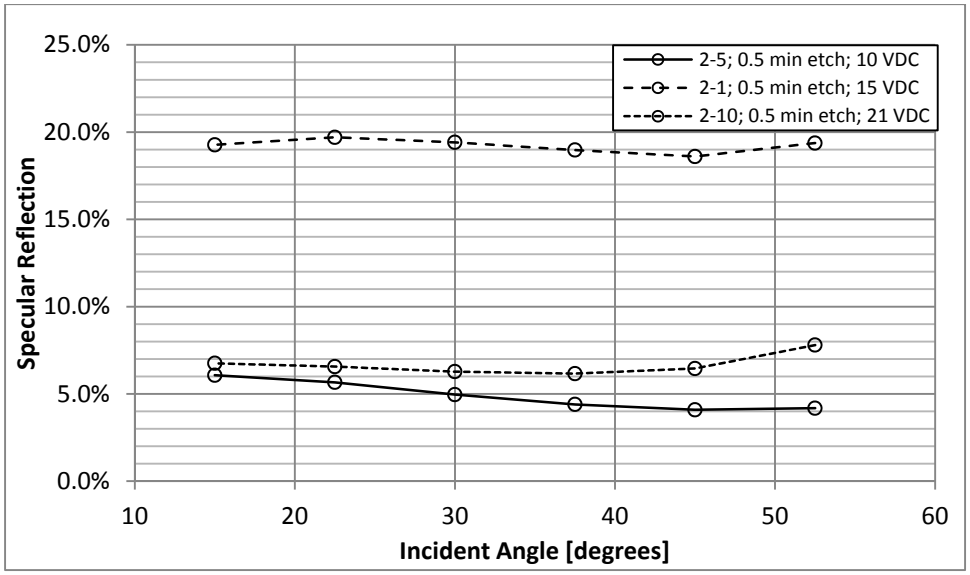

Figures 3.17, 3.18, and 3.19 show that the incident beam angle has little effect on specular reflectance measurements when varied from 15 to 52.5°. This is most evident in Figure 3.17 for the samples etched for 20 minutes; any angular dependence is within the error established during the centerpoint comparison. Figures 3.18 and 3.19 show a ~1% change on each sample as incident angle varies. However, this change is small. Also, consistent trends between samples are not apparent.

Chapter 4 - Discussion

The anodization process conducted at each of the experimental conditions led to a significant decrease in specular reflectivity. This is apparent by comparing the measurements recorded for the mirror and non-anodized samples in Figure 3.8 with the measurements reported for the anodized samples presented in Chapter 3. Quantitatively at a 13.1% acceptance angle, the specular reflectivity decreased from ~70% on the non-anodized samples to a range between 1.2% and 20.6% for anodized samples dependent on the process conditions. This 49.4 to 68.8% reduction in specular reflectance represents a significant shift in the optical performance of the aluminum surface and has the potential to have a large impact on DLC's optical design and development processes.

The decrease in specular reflectance does not distinguish between an increase in diffuse scatter and a loss in total reflectance. In a previous study, Shih et al.[6] reported a decrease in total reflectance from 85 to 75% after a 5 minute anodization process. This decrease is attributed to an increase in the alumina layer's ability to absorb light as its thickness increases. It is likely that some fraction of the specular reflection decrease is due to the absorption in the alumina layer. Whether or not the absorption characteristics are constant between samples or vary per test condition cannot be distinguished with the test methods presented in Chapter 2. Fortunately, for the purposes of laser module design making this distinction is not necessary, as the overall decrease in specular reflectance, through absorption or scattering, is the desired effect.

Etch Time Effect on Specular Reflectivity

There is a strong correlation between etch time and decreasing specular reflectivity. Figure 4.1 summarizes the results for measurements corresponding to a 13.1° acceptance angle and an incident angle of 45°. The figure shows the most dramatic decrease in specular reflectivity between the 0.5 and 5 minute test conditions where the 10, 15, and 21 volt conditions yield a specular reflectivity decrease of 4.9, 15.3, and 6.4%, respectively.

Figure 4.1: Specular Reflection vs. Etch Time

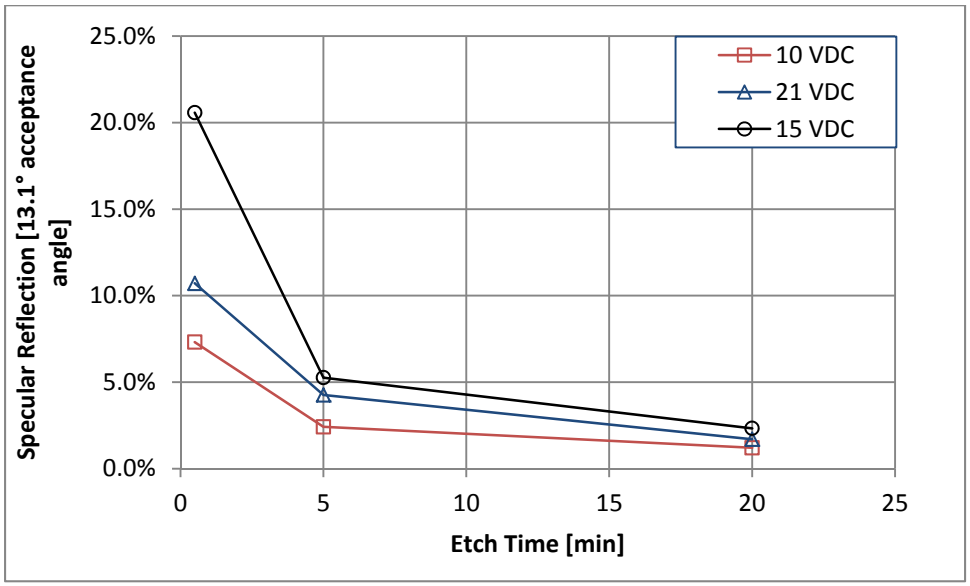

The trend shown in Figure 4.1 is consistent with previous work by Beck and Funk[15] who showed a similar trend for gloss measurements on aluminum and aluminum alloys. In their study, a 20 minute etch process resulted in a gloss decrease from ~60 to a minimum of 20 gloss units. The loss is correlated to an increase in roughness, $\Delta R = 5$ µm, at the aluminum surface. The authors proposed that the roughness was not significantly affected by the subsequent growth of the alumina layer and that enough incident light traveled through the layer to scatter off of the bulk aluminum and decrease the gloss measurements.

Anodization Potential Effect on Specular Reflectivity

The effect of anodization potential on specular reflectivity shown in Chapter 3 does not correlate well with previous work. Cochran and Keller[24] (as cited by Wernick[3]) show that image clarity decreases with anodization potential. Their work, conducted on several aluminum alloys under nearly identical anodization conditions, suggests that a 10 to 12 volt potential would produce a brighter, more specularly reflective surface than higher potentials. In contrast, the results from Chapter 3 show that samples produced at 15 volts demonstrate a maximum specular reflectivity.

The mechanism responsible for a 15 volt potential producing samples with the highest specular reflectivity is not well understood. The optical properties of the alumina layer are reported to depend on the surface roughness, chemical composition, and the structural

characteristics (e.g. cell and pore diameters) of the layer.[6] Since the alumina growth step has a negligible effect on surface roughness[6] and the chemical composition is held constant within the experimental parameters, it can be inferred that the alumina structural properties are the primary factor affecting the specular reflectance. As shown previously in Figure 1.6, the cell and pore diameters within the alumina layer appear to increase linearly with anodization potential between 10 and 20 volts.[18] However, the specular reflectance measurements shown in Figures 3.14 and 3.15 display a maximum at the 15 volt condition, suggesting a relationship with alumina layer structure other than cell and pore diameter.

Angular Dependence of Specular Reflectivity

The assertion that specular reflectivity is a function of the reflection angle of the incident light, $I/I_o = f(\theta_i)$, made in the model published by Beckmann and Spizzichino[5], conflicts with the measurements presented in Figures 3.17, 3.18, and 3.19. The figures show that the incident angle has little influence on the specular reflectance between 15° and 52.5°. For the samples produced at the 0.5 and 5 minute etch times, the specular reflectance changed ~1% as the incident angle varied. Additionally, for samples produced with a 20 minute etch time, the angular dependence of the specular reflectivity decreased to a point where it became indistinguishable from the sample-to-sample variances. As discussed in Chapter 1, the model, shown in Equation 2, cannot be directly applied since the anodized surface violates the model's ideal conductor assumption. However, the measurements presented in Figures 3.17 through 3.18 suggest that not only is the model invalid, but that incident angles between 15° and 52.5° do not significantly affect the specular reflectance of anodized surfaces prepared as described in Chapter 2.

Chapter 5 - Conclusion

Anodizing causes a significant shift in the optical performance of an aluminum surface and will lead to an improvement in DLC laser module design. Specifically, anodizing polished 6061-T6 aluminum alloy to a MIL-A-8625, Class II, Type I standard reduces the specular reflectance of the surface. When tested with a 660 nm collimated laser source and a 13.1° acceptance angle on the detector, the specular reflectance decreased from ~70% to between 20.6% and 1.2%, depending on the process conditions. This reduction, when applied to surfaces adjacent to the optical pathway in a DLC laser module design will decrease the intensity of stray light and associated undesirable image artifacts.

A decrease in specular reflectivity is observed as the etch process time increased from 0.5 to 20 minutes. The magnitude of the decrease was significant, ranging from 18.3 to 6.1% when measured with a 13.1° acceptance angle. The specular reflectance also correlated with the characteristic potential profiles achieved during the alumina growth process. Samples produced with a process potential of 15 volts consistently had greater specular reflectivity than those produced with process potentials of 10 or 21 volts. Overall, the reduction in specular reflectance was impacted more significantly by etch process time than by potential during alumina layer growth. This was most evident for 20 minute etch times where the maximum specular reflectance measured <2.5% when compared to about 70% for unprocessed samples.

Anodization will be an effective means to decrease specular reflections and reduce the impact of stray light artifacts in a DLC laser module. Specification of a >5 minute etch process time, under conditions similar to those evaluated, will result in the desired specular reflectance reduction. Further reductions could be achieved by increasing the etch time to 20 minutes or altering the potential during anodic alumina layer formation. Additional effort will be necessary to establish optimal process conditions that take into account the unique capabilities of anodization service providers.

Chapter 6 - References

1. Hecht, Eugene. *Optics; Third Ed.;* Addison-Wesley Longman, Inc, 1998.

2. Peiponen, K.; Myllyia, R.; Priezzhev, A. V. *Optical Measurement Techniques: Innovations for Industry and the Life Sciences;* Verlag Berlin Heidelberg: Springer, 2010.

3. Wernick, S.; Pinner, R.; Sheasby, P. G. *The Surface Treatment and Finishing of Aluminum and its Alloys;* Finishing Publications Ltd., 1987.

4. Alexander-Katz, R.; Barrera, R. G**.** Surface Correlation on Gloss**.** *Journal of Polymer Science: Part B: Polymer Physics*. **1998**, 36, 1321-1334.

5. Beckmann, P.; Spizzichino, A. *The Scattering of Electromagnetic Waves from Rough Surfaces;* Artech House, 1987.

6. Shih, T.; Wei, P.; Huang, Y. Optical properties of anodic aluminum oxide films of A11050 alloys. *Surf. Coat. Technol.* **2008**, 202, 3298-3305.

7. US Navy. Military Specification: Anodic Coatings for Aluminum and Aluminum Alloys. Mil-A-8625F; Amendment 1. 2003.

8. Corcoran, B. Introduction to the Science and Engineering of Hardcoat Anodizing. *Aluminum Hardcoat Anodizing Seminar*, LightMetal Industries, LLC, Unpublished work, 2009.

9. Thompson, G. E.; Habazaki, H.; Shimizu, K.; Sakairi, M.; Skeldon, P.; Zhou, X.; Wood, G. C. Anodizing of Aluminum Alloys. *Aircr. Eng. Aerosp. Tech.* **1999**, 71, 228-238.

10. Feliu, S. Jr.; González, J. A.; López, V.; Bartolome, M. J.; Escudero, E.; Otero, E. Characterization of Porous and Barrier Layers of Anodic Oxides on Different Aluminum Alloys. *J. Appl. Electrochem.* **2007**, 37, 1027-1037.

11. Tsangaraki-Kaplanoglou; Theohari, S.; Dimogerontakis, Th.; Wang, Y.; Kuo, H.; Kia, S. Effect of Alloy Types on the Anodization Process of Aluminum. *Surf. Coat. Technol.* **2006**, 200, 5634-2641.

12. International Alloy Designations and Chemical Composition Limits for Wrought Aluminum and Wrought Aluminum Alloys. *Registration Record Series Teal Sheets.* Arlington, VA: The Aluminum Association, Inc., 2009.

13. Stepiowski, W. J.; Zasada, D.; Bojar, Z. First Step of Anodization Influences the Final Nanopore Arrangement in Anodized Alumina. *Surf. Coat. Technol*. **2011**, 206, 1416-1422.

14. Beck, G.; Petrikowski, K. Influence of the Microstructure of the Aluminum Substrate on the Regularity of the Nanopore Arrangement in an Alumina Layer Formed by Anodic Oxidation. *Surf. Coat. Technol.* **2008**, 202, 5084-5091.

15. Beck, G.; Funk, S. Correlation Between Optical Appearance and Orientation of Aluminum. *Surf. Coat. Technol.* **2012**, 206, 2371-2379.

16. Aerts, T.; De Graeve, I.; Terryn, H. Anodizing of Aluminum Under Applied Electrode Temperature: Process Evaluation and Elimination of Burning at High Current Densities. *Surf. Coat. Technol*. **2010**, 204, 2754-2760.

17. Yu, C.; Hu, C.; Bai, A.; Yang, Y. Pore-size Dependence of AAO Films on Surface Roughness of AL-1050 Sheets Controlled by Electropolishing Coupled with Fractional Factorial Design. *Surf. Coat. Technol*. **2007**, 201, 7259-7265.

18. Ono, S.; Masuko, N. Evaluation of Pore Diameter of Anodic Porous Films Formed on Aluminum. *Surf. Coat. Technol.* **2003**, 169-170, 139-142.

19. Rao, C. B.; Raj, B. Study of Engineering Surfaces Using Laser-Scattering Techniques. *Sadhana*. **2003**, 28, 739-761.

20. Swann, E. D.; Thomas, R. W. (unpublished). 1951.

21. Staubwasser, P. Influence of the Structure on the Decorative Appearance of Anodised AlMgSi0.5 Profiles. Ph.D Dissertation. RWTH Aachen, 1990.

22. Ono, S.; Saito, M.; Ishiguro, M.; Asoh, H. Controlling Factor of Self-Ordering of Anodic Porous Alumina. *J. Electrochem. Soc.* **2004**, 151, B473-B478.

23. Vrublevskya, I.; Parkouna, V.; Schreckenbach, J.; Marx G. Study of Porous Oxide Film Growth on Aluminum in Oxolic Acid Using Re-Aaodizing Technique. *Appl. Surf. Sci.* **2004**, 227, 282-292.

24. Cochran, W. C.; Keller, F. *Proceedings of the American Electroplaters Society.* **1961**, 48, 82-89.